OUKA
The University of Osaka
Institutional Knowledge Archive

Title	Studies on Functionalization of Stimuli-Responsive Network Materials Based on Cellulose through Morphology Control
Author(s)	Roopsung, Nontarin
Citation	大阪大学, 2023, 博士論文
Version Type	VoR
URL	https://doi.org/10.18910/92934
rights	
Note	

The University of Osaka Institutional Knowledge Archive : OUKA

https://ir.library.osaka-u.ac.jp/

The University of Osaka

Doctoral Dissertation

Studies on Functionalization of Stimuli-Responsive Network Materials Based on Cellulose through Morphology Control

セルロースを基盤とした刺激応答性ネットワーク材料の形態制御による機能化に関する研究

Nontarin Roopsung

June 2023

Graduate School of Engineering
Osaka University

Table of Contents

Page

General Introduction **1**

References 10

Chapter 1 **14**

Stiffness-Changing Materials with Shape Stability Based on Cellulose Monolith and Poly(stearyl methacrylate)

1-1. Introduction 14

1-2. Experimental Section 16

1-3. Results and Discussion 19

1-4. Conclusions 29

1-5. References 30

Chapter 2 **33**

Switchable Stiffness of Bacterial Cellulose Composite Reinforced with Thermoresponsive Phase-Change Particles

2-1. Introduction 33

2-2. Experimental Section 34

2-3. Results and Discussion 36

2-4. Conclusions 41

2-5. References 42

Chapter 3 **44**

Hydrogel Actuators with Gradient Distribution of Cellulose Nanocrystals for Controllable Bending Properties

3-1. Introduction 44

3-2. Experimental Section 45

3-3. Results and Discussion 49

3-4. Conclusions 57
3-5. References 59

Concluding Remarks 62

List of Publications 64

Acknowledgements 65

General Introduction

Stimuli-responsive materials

Stimuli-responsive materials are smart materials which can undergo the physical or chemical changes on receiving external stimuli. These changes are accompanied by differences on the properties of the stimuli-responsive polymers in different environmental conditions.[1] These polymers can respond to various stimuli, such as a variation in temperature,[2,3] chemical composition,[4,5] and mechanical force,[6–8] or stimulated by exposure to light[9–11] or electric[12,13] and magnetic fields[14–16] (**Figure 1**). Such responsiveness especially in engineered polymer is demonstrated by triggering microscopic conformational transitions and amplifying them into macroscopically measurable changes.[17,18] These materials gained tremendous attention in scientific research and technology and are extensively manufactured for a wide variety of applications, such as variable stiffness composite that create a favorable load distribution;[19] soft robot locomotive skin that is realized by selectively controlling the particle jamming;[20] composite materials that actuate and mimic the action of muscles;[21] soft manipulator from smart flexible responsive hydrogel that shows fast and controllable light-driven bending behavior;[22] and force sensor that is utilized by stiffness change of material based on the temperature.[23]

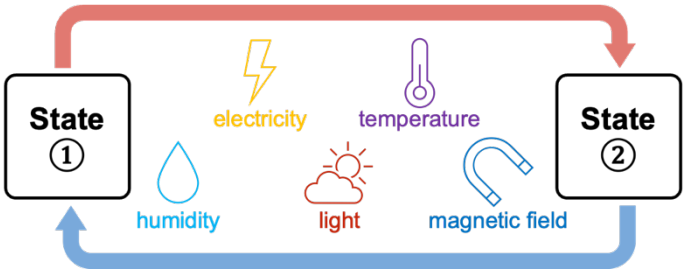

Figure 1. Conceptual illustration of stimuli-responsive materials experiencing a change in state of material in response to external stimuli.

The responsiveness of these materials derived from responsive polymer should be modifiable in response to external stimuli in order to trigger switchable interaction or conformational changes, including cross-linking by dynamic covalent bonds or non-covalent interactions,[24,25] phase and glass transition of thermoplastics,[26,27] polymer vitrification,[28] and supercooling material.[29,30] In triggering these changes in polymer, the external stimuli disturbed an equilibrium involving polymer-solvent and polymer-polymer interactions and steered it towards a new equilibrium in which the conformation of the polymer shifts.[17] The microscopic changes, which manifested as a large macroscopic change, correspondingly produced a distinct conformational shape, which in

consequently enabled to the mechanical stability of the structure. However, maintaining its structural stability during external stimuli-induced changes is essential, due to the fracture is generated by the fact that the responsive part, by itself, lacked the requisite toughness to sustain the structure, Additionally, for high-performance applications, these materials should have moduli exceeding 1 GPa, with combination of high strength, high fracture toughness, and excellent impact performance.[31] Traditionally, there was a trade-off relationship between structural performance and durability, as their stiffness and strength tended to be fractured upon impact, whereas more ductile responsive polymeric materials typically had a lower yield strength.[32,33] The primary method of solving these problems is to design network structures by incorporating stable components and networks that improve the impact resistance of the systems,[34] including thermoplastic additives[35,36] and inorganic[37,38] and rubber particles.[33,39] Therefore, to develop an effective stimuli-responsive material, the architecture of the material should bridge the disparity between mechanical stability and responsiveness (**Figure 2**).

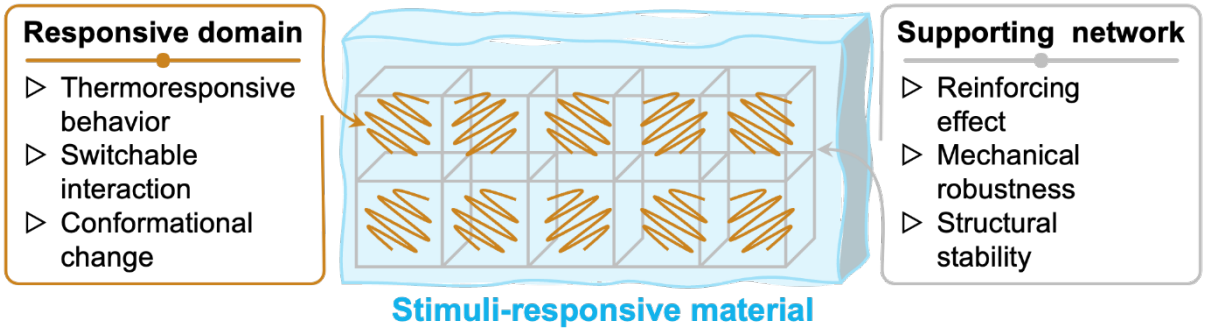

Figure 2. A supporting network and a responsive domain as the prerequisites for stimuli-responsive materials.

Cellulose

Cellulose is the most abundant renewable biopolymer on Earth and the fundamental structural component of plant cell walls (**Figure 3**). In addition to plants, green algae, fungi, bacteria, and tunicates (small and sessile marine animals) can be also used as the sources of cellulose production.[40,41] Its molecular formula is $(C_6H_{10}O_5)_n$, where n is the degree of polymerization and reflects the number of anhydrous glucose unit (AGU), widely differing from

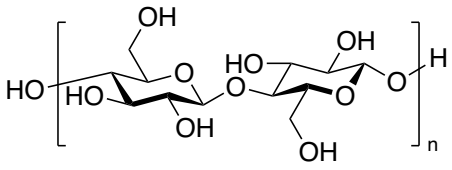

Figure 3. Basic chemical structure of cellulose exhibiting the cellobiose repeat unit (n = DP, degree of polymerization).

hundreds to tens of thousands.[42] As a result, cellulose is an extensive, linear-chain polymer with a large number of hydroxyl groups (three per AGU), comprised of β-D-glucopyranose units interconnected by β-1-4-glycosidic linkages, present in the thermodynamically preferred $^4C_1$ conformation.[43] Correspondingly, it is abundantly clear that these hydroxyl groups and their capacity to establish hydrogen bonds play a prominent role in dominating the crystalline packing and influencing the physical properties of cellulose.[44] The cellulose microfibril is the basic structural component of cellulose, formed during the biosynthesis. Cellulose biogenetically forms a fibril in which a long thread-shaped bundle of molecules is laterally stabilized by intermolecular hydrogen bonds.[45] Each microfibril comprises of a string of cellulosic crystalline attached by unstructured amorphous regions along the microfibril axis,[46] such as twists and kinks.[47] Depending on its source and subsequent processing, cellulose fibers can assemble into a variety of crystalline structures.

The molecular structure imparts cellulose with its characteristic properties: hydrophilicity, chirality, degradability, and broad chemical variability derived from the hydrogen bond donor ability of the hydroxyl groups. Cellulose microfibrils have become increasingly prevalent as reinforcing materials in polymeric composites owing to environmental concerns.[48] Cellulose microfibrils display environmental friendliness and exceptional mechanical strength. Reportedly, they range between 78 and 114 GPa.[49,50] Since cellulose is the basis for extensive hydrogen bond networks, which give cellulose a multitude of partially crystalline fiber structures and morphologies, it has been exploited as reinforcement materials for composites with diverse morphological control, comprising cellulose monolith, bacterial cellulose nanocrystal network, and cellulose nanocrystals.

Cellulose monolith

Monoliths are single-piece porous stationary phase materials that are commonly beneficial for separation techniques such as gas and liquid chromatography, high-performance liquid chromatography, and capillary electrochromatography.[51,52] In opposed to typical porous beads, the benefits of monoliths include their mechanical durability, low cost, and simplicity of *in situ* manufacturing, lack of void volume, adjustable pore size, and simple functionalization for use in ion-exchange, affinity, and mixed operations.[53] Another benefit of monoliths is that they can be conveniently formed into many shapes, including capillary, column, micropipette tip, and

tubular.[54] Owing to these advantages for chromatographic techniques, monoliths can be utilized as other fields of application, including thermal insulating organic foam with enhanced porosity and flexible feature;[55] energy absorber or cushion from polymeric foams exhibiting high stiffness and excellent recoverable compressibility;[56] thermal energy monolithic storage displaying extremely high heat capacity;[57] and ion exchange monoliths employed for the removal of cationic and anionic dyes.[58] These applications suggested that the mechanical properties were taken into account to be modified and then achieve the desired mechanical stability.

Recently, three forms of monolithic material fabrication are being studied: inorganic monoliths, organic monoliths, and organic-inorganic hybrid monoliths. The organic monoliths are comprised of organic polymers, which can be chiefly divided into methacrylate- and acrylate-based polymer groups.[59] They advanced from the brittle inorganic counterparts by becoming more flexible and tougher while retaining their natural shape.[60] Cellulose monolith (CM) is promising alternatives among them due to facile modifiability, biocompatibility, simple preparation process, and chemical and physical stability. Xin *et al.*[61] reported a thermally induced phase separation (TIPS) techniques that is used as a novel route for the preparation of cellulose monolith by selecting cellulose acetate as the starting material. This monolith exhibited a continuous macropore with a rough surface and a hydrophilic feature that permitted for simple and extensive modification. It illustrates that CM can be used for various field of applications, thanks to the advantages of monolith with unique morphologies, serving as stable networks.

Bacterial cellulose

Bacterial cellulose (BC) is primarily synthesized in static cultivation by bacteria such as *Acetobacter G. xylinus* species, referred to as a high-water-content biocompatible hydrogel.[62] BC hydrogel is a natural hydrogel architecture with ribbon-shaped ultrafine nanofibrils of cellulose assembled by intermolecular and intramolecular hydrogen bonds to maintain a three-dimensional network. In addition, BC exhibits various distinctiveness such as high purity lacking lignin and hemicellulose, large surface area and aspect ratio, high porosity, relatively large retention capacity, outstanding mechanical strength, and high crystallinity, which creates new prospects for a multitude of applications including biomedicine.[63,64]

Recently, there has been substantial potential in the BC-based synthesis of stimuli-responsive hydrogel. Pedige *et al.*[65] developed a mechanically adaptive hydrogel composite under different

pH from BC and chitosan fiber. This exhibited adaptable mechanical strength in response to pH with maintaining three-dimensional stability. Wang *et al.*[66] demonstrated composite hydrogel prepared from BC and poly(*N*-isopropylacrylamide) (PNIPAAm) by a simple *in situ* polymerization process. It was found that the hydrogel could swell and shrink in the axial perpendicular to the layers in response to temperature, supporting that BC can be utilized for strengthening the network with remaining responsiveness. These composite models were constructed based on the mechanical stability of stimuli-responsive hydrogel, highlighting that the BC network functions as a stable network in stimuli-responsive materials.

Cellulose nanocrystal

Cellulose nanocrystals (CNCs) are crystalline nanoparticles derived from cellulose that are crucial to produce novel bio-based materials with its characteristics. They are a potential nanocomposite reinforcement agent due to their low density (1.6 g mL^{-1}), high strength (10 GPa),[46] and high modulus (143 GPa).[67] They are applicable for the manufacturing of biomedical devices, implants, and textile materials since they are non-toxic, biocompatible, and abundantly available worldwide.[40,46] CNCs consist of rod-like cellulose crystals with widths of 5-70 nm and lengths between 100 nm to several micrometers, depending on the natural cellulosic sources and preparation methods.[68] Acidic hydrolysis was conventionally used to produce CNC suspension by eliminating the amorphous regions of purified cellulose and retaining the crystalline regions. In general, sulfuric and hydrochloric acids were the most frequently employed for this purpose. The abundance of charged sulfate on the surface of water facilitated the dispersion of CNCs produced by sulfuric acid hydrolysis.

The usage of CNCs for diverse purposes can be classified into two major categories: the use of functionalized or as-synthesized CNC and the use of polymeric nanocomposites in which CNC behaves as a reinforcing agent. A polymer nanocomposite is a multiphase material in which the polymer phase is reinforced with nanostructures, with the greater surface area of the reinforcing material conferring unique characteristics. Gevorkian *et al.*[69] prepared the nanocolloidal hydrogel, obtained from CNCs and methacryloyl gelatin, exhibiting stimuli-triggered shape transformation solely due to structural anisotropy.[69] It was shown that the change in shape was reliant on the distribution of CNCs in each region of the patterning hydrogel, indicating that CNCs

can be employed as the reinforcing agent in the composite hydrogel and as a means of enhancing the dimensional support of hydrogel with stimuli-responsiveness.

Thermoresponsive polymers

Responsive polymers, used as the responsive domain in stimuli-responsive materials, are the polymer which responds to the external stimuli by altering its physicochemical properties. Such polymers have found many applications in the biomedical and industrial fields. Among the multitude of responses to external stimuli as aforementioned, the most studied and applicable response is temperature due to ease of controllability and broad designability.[70] Thermoresponsive polymer exhibited the microscopic change, such as crystalline/melting, isotropic/anisotropic, and globular/swollen transition, and supramolecular association/dissociation.

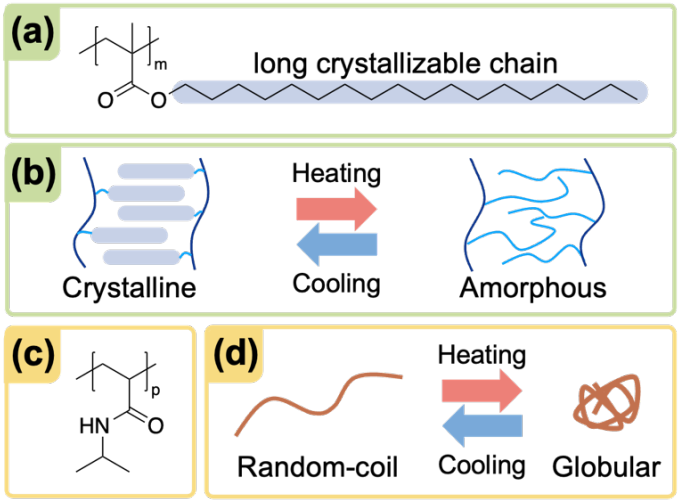

Figure 4. (a, c) Chemical structures and (b, d) their transition in response to temperature of PSMA and PNIPAAm, respectively.

Poly(stearyl methacrylate) (PSMA) is a comb-type polymer with an 18-carbon aliphatic chain, rendering it a polymer with a crystallizable side-chain. Its side chain can construct a crystalline structure from a dense packing conformation, producing a sharp phase change that enable a large modulus shift from rigid (~100 MPa) to soft (~100 kPa) (**Figure 4a and b**). Even through a rapid phase transition, the dangling side chain is fast moving and uniform in length, permitting for a narrow phase transition span. Also, by varying the number of carbon atoms in the side chain of *n*-alkyl methacrylates or acrylates monomers, the specific melting point of this polymer can be controlled within a broad range.[71]

Poly(*N*-isopropylacrylamide) (PNIPAAm) is a most extensively studied polymer exhibiting lower critical solution temperature (LCST) at 32 °C, which is close to physiological temperature.[72] As the solution temperature increased beyond the LCST, the conformation of the polymer transformed from solvated random coil to desolvated globular structure (**Figure 4c and d**). This transition can be thermodynamically modulated by varying the hydrophilicity-based

polymer composition.[73] Transition of PNIPAAm in response to temperature can be promisingly utilized in stimuli-responsive materials.

Material design of stimuli-responsive materials in this thesis

In this thesis, the author developed stimuli-responsive materials combining cellulose-based materials as supporting network and thermoresponsive polymers as responsive domain to achieve the desirable function of the materials. The morphologies of network in the materials were controlled based on the mechanical stability required in the functional stimuli-responsive materials. In chapter 1, the author fabricated the stiffness-changing monolithic composite by using CM and PSMA as a phase-changing thermoresponsive polymer. The stiffness-changing behavior was enhanced by creating intermingled structure constructed from PSMA and backbone of CM. Additionally, the monolithic composite exhibited recoverable compressibility. In chapter 2, the author prepared the composite hydrogel based on BC and PSMA. This composite material displayed the thermoresponsive change in stiffness, influenced from PSMA particles distributed in BC network as a stiff-reinforcing filler. Furthermore, in chapter 3, the author constructed the hydrogel actuator from PNIPAAm and CNC, which was gradiently distributed in PNIPAAm network *via* electrophoretic technique. The gradient structure of CNC was optimized by facilely adjusting the fabrication condition. The actuating characteristics was evaluated from bending behavior, directly impacted from gradient structure of CNC.

Outlines of this thesis

In this doctoral thesis, the author presented functional stimuli-responsive materials based on thermoresponsive polymers and cellulosic components with various types of morphological control. The materials demonstrated the stiffness-switching behavior (Chapter 1 and 2) and actuating feature as bending behavior (Chapter 3) in response to different temperature. This thesis is anticipated to promote the industrial usefulness of functional stimuli-responsive materials such as soft robotic components, shape memory materials, force sensors, and actuators.

Chapter 1

In chapter 1, the author fabricated a stiffness-changing monolithic materials, comprising of cellulose monolith (CM)as stable supporting network and PSMA as responsive domain, in order

to exhibit stiffness change in response to temperature with maintaining the dimensional stability of the material (**Figure 5**). CM was modified with acryloyl (AC) group. The monolithic composite was prepared via polymerization of SMA monomer with the presence of AC-modified CM. PSMA showed the crystallization/melting phase transition with changing temperature, rendering the stiffness-switching of the monolith. Moreover, shape recoverability and reversibility of the thermoresponsive stiffness change was evaluated.

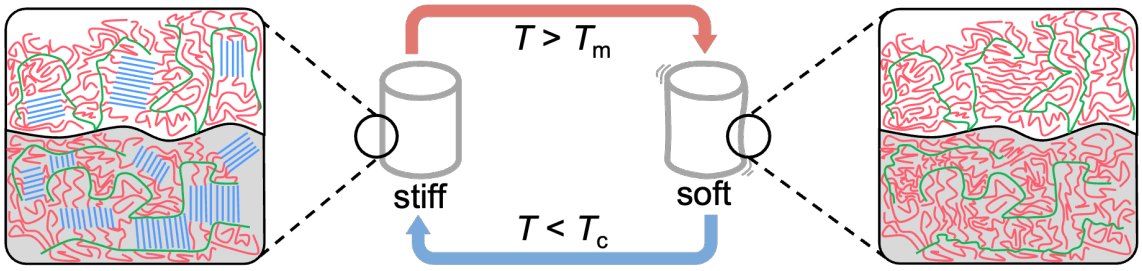

Figure 5. Conceptual illustration of the stiffness-changing monolithic materials.

Chapter 2

In chapter 2, composite hydrogels with thermoresponsive stiffness were prepared using bacterial cellulose (BC) as a supporting network of nanofiber with incorporation of PSMA particles acting as the stiffness-changing filler (**Figure 6**). BC was modified with AC group and PSMA was subsequently polymerized in the BC network. As a result of particle production, its distribution in a BC network deriving from diverse polymerization conditions was examined as an effect on temperature responsiveness. It was observed that the amount of PSMA particles in the BC network had an influence on responsiveness, which increased with the amount of PSMA incorporated into the BC network.

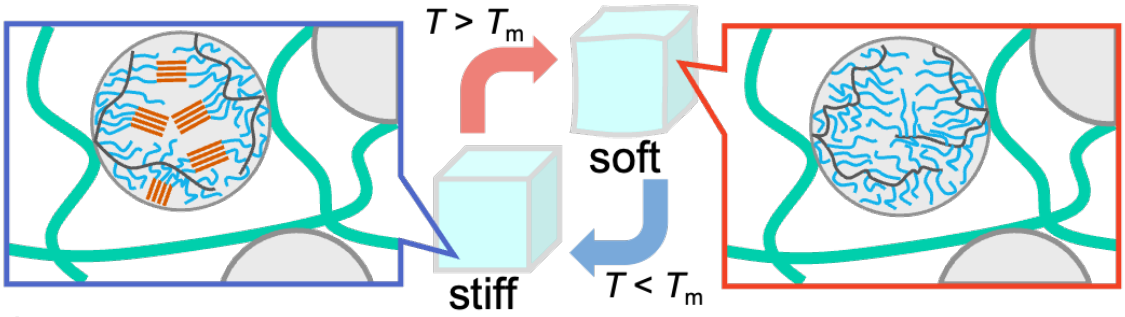

Figure 6. Conceptual illustration of thermoresponsive hydrogels with PSMA particles distributed in the BC network.

Chapter 3

In chapter 3, using electrophoretic method, thermoresponsive single-layer hydrogel actuators were constructed from a PNIPAAm network and gradient structure of CNC (**Figure 7**). By adjusting the preparation conditions, the gradient distribution of CNC was controlled to enhance the bending angle and response speed. Additionally, CNCs with different dimension was incorporated as the gradient component to investigate the optimum properties of the CNC-rich layer for the actuation behavior.

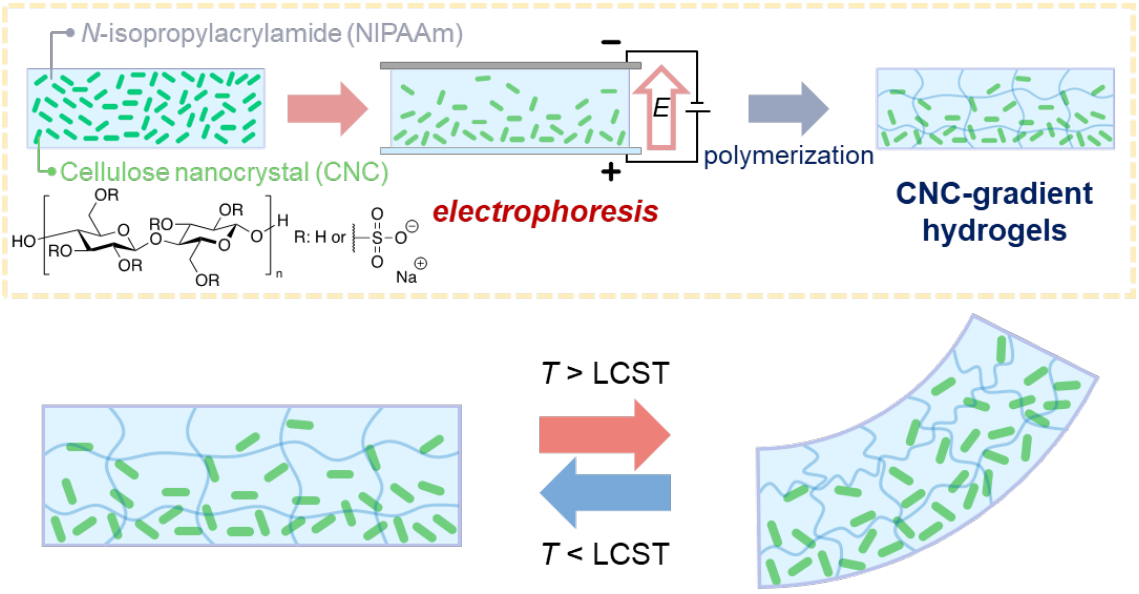

Figure 7. Conceptual illustration of gradient nanocomposite hydrogels.

References

[1] M. A. C. Stuart, W. T. S. Huck, J. Genzer, M. Müller, C. Ober, M. Stamm, G. B. Sukhorukov, I. Szleifer, V. V. Tsukruk, M. Urban, F. Winnik, S. Zauscher, I. Luzinov, S. Minko, *Nat Mater* **2010**, *9*, 101.

[2] H. Gu, G. Wang, X. Cao, *J Appl Polym Sci* **2021**, *138*, 51509.

[3] M. S. A. Abdelaty, *J Polym Environ* **2021**, *29*, 3227.

[4] X. Peng, Q. Peng, M. Wu, W. Wang, Y. Gao, X. Liu, Y. Sun, D. Yang, Q. Peng, T. Wang, X. Z. Chen, J. Liu, H. Zhang, H. Zeng, *ACS Appl Mater Interfaces* **2022**, *15*, 19560.

[5] Y. Feng, M. Taraban, Y. B. Yu, *Soft Matter* **2012**, *8*, 11723.

[6] Y. Sagara, M. Karman, A. Seki, M. Pannipara, N. Tamaoki, C. Weder, *ACS Cent Sci* **2019**, *5*, 874.

[7] Y. Sagara, M. Karman, E. Verde-Sesto, K. Matsuo, Y. Kim, N. Tamaoki, C. Weder, *J Am Chem Soc* **2018**, *140*, 1584.

[8] K. Hiratsuka, T. Muramatsu, T. Seki, C. Weder, G. Watanabe, Y. Sagara, *J Mater Chem C Mater* **2023**, *11*, 3849.

[9] Z. L. Pianowski, J. Karcher, K. Schneider, *Chemical Communications* **2016**, *52*, 3143.

[10] I. N. Lee, O. Dobre, D. Richards, C. Ballestrem, J. M. Curran, J. A. Hunt, S. M. Richardson, J. Swift, L. S. Wong, *ACS Appl Mater Interfaces* **2018**, *10*, 7765.

[11] K. P. Sonu, L. Zhou, S. Biswas, J. Klier, A. C. Balazs, T. Emrick, S. R. Peyton, *Langmuir* **2022**, *39*, 2659.

[12] A. Venkataraman, E. V. Amadi, Y. Chen, C. Papadopoulos, *Nanoscale Res Lett* **2019**, *14*, 220.

[13] B. W. Walker, R. Portillo Lara, E. Mogadam, C. Hsiang Yu, W. Kimball, N. Annabi, *Prog Polym Sci* **2019**, *92*, 135.

[14] S. Louguet, B. Rousseau, R. Epherre, N. Guidolin, G. Goglio, S. Mornet, E. Duguet, S. Lecommandoux, C. Schatz, *Polym Chem* **2012**, *3*, 1408.

[15] S. Ghosh, T. Cai, *J Phys D Appl Phys* **2010**, *43*, 415504.

[16] Z. Li, J. Shen, H. Ma, X. Lu, M. Shi, N. Li, M. Ye, *Polymer Bulletin* **2012**, *68*, 1153.

[17] D. Wandera, S. R. Wickramasinghe, S. M. Husson, *J Memb Sci* **2010**, *357*, 6.

[18] F. Liu, M. W. Urban, *Progress in Polymer Science (Oxford)* **2010**, *35*, 3.

[19] M. Iragi, C. Pascual-González, A. Esnaola, U. Morales, J. Aurrekoetxea, C. S. Lopes, L. Aretxabaleta, *Addit Manuf* **2023**, *63*, 103418.

[20] Y. Wei, Y. Chen, T. Ren, Q. Chen, C. Yan, Y. Yang, Y. Li, *Soft Robot* **2016**, *3*, 134.

[21] I. H. Kim, S. Choi, J. Lee, J. Jung, J. Yeo, J. T. Kim, S. Ryu, S. K. Ahn, J. Kang, P. Poulin, S. O. Kim, *Nat Nanotechnol* **2022**, *17*, 1198.

[22] Z. Sun, C. Song, J. Zhou, C. Hao, W. Liu, H. Liu, J. Wang, M. Huang, S. He, M. Yang, *Macromol Rapid Commun* **2021**, *42*, 2100499.

[23] K. Takashima, H. Kamizono, M. Takenaka, T. Mukai, *ROBOMECH Journal* **2017**, *4*, 17.

[24] J. H. Xu, S. Ye, J. J. Fu, *J Mater Chem A Mater* **2018**, *6*, 24291.

[25] C. Qian, T. A. Asoh, H. Uyama, *J Mater Chem B* **2020**, *8*, 2400.

[26] B. Yetiskin, O. Okay, *ACS Appl Polym Mater* **2022**, *4*, 5234.

[27] K. Sato, T. Nakajima, T. Hisamatsu, T. Nonoyama, T. Kurokawa, J. P. Gong, *Advanced Materials* **2015**, *27*, 6990.

[28] L. Chen, C. Zhao, J. Huang, J. Zhou, M. Liu, *Nat Commun* **2022**, *13*, 6821.

[29] B. S. Chang, R. Tutika, J. Cutinho, S. Oyola-Reynoso, J. Chen, M. D. Bartlett, M. M. Thuo, *Mater Horiz* **2018**, *5*, 416.

[30] F. (Kuo) Yang, A. Cholewinski, L. Yu, G. Rivers, B. Zhao, *Nat Mater* **2019**, *18*, 874.

[31] E. Grossman, I. Gouzman, *Nucl Instrum Methods Phys Res B* **2003**, *208*, 48.

[32] E. Crawford, A. J. Lesser, *J Polym Sci B Polym Phys* **1998**, *36*, 1371.

[33] E. D. Bain, D. B. Knorr, A. D. Richardson, K. A. Masser, J. Yu, J. L. Lenhart, *J Mater Sci* **2016**, *51*, 2347.

[34] T. R. Long, R. M. Elder, E. D. Bain, K. A. Masser, T. W. Sirk, J. H. Yu, D. B. Knorr, J. L. Lenhart, *Soft Matter* **2018**, *14*, 3344.

[35] K. A. Masser, D. B. Knorr, M. D. Hindenlang, J. H. Yu, A. D. Richardson, K. E. Strawhecker, F. L. Beyer, J. L. Lenhart, *Polymer (Guildf)* **2015**, *58*, 96.

[36] J. L. Hedrick, I. Yilgor, M. Jurek, J. C. Hedrick, G. L. Wilkes, J. E. McGrath, *Polymer (Guildf)* **1991**, *32*, 2020.

[37] E. Bugnicourt, J. Galy, J. F. Gérard, H. Barthel, *Polymer (Guildf)* **2007**, *48*, 1596.

[38] J. Z. Liang, *J Appl Polym Sci* **2002**, *83*, 1547.

[39] R. Bagheri, B. T. Marouf, R. A. Pearson, *Polymer Reviews* **2009**, *49*, 201.

[40] M. M. De Souza Lima, R. Borsali, *Macromol Rapid Commun* **2004**, *25*, 771.

[41] A. C. O'sullivan, *Cellulose* **1997**, *4*, 173.

[42] A. Blanco, M. C. Monte, C. Campano, A. Balea, N. Merayo, C. Negro, In *Handbook of Nanomaterials for Industrial Applications*, Elsevier, **2018**, pp. 74–126.

[43] D. Klemm, B. Heublein, H. P. Fink, A. Bohn, *Angewandte Chemie - International Edition* **2005**, *44*, 3358.

[44] M. J. John, S. Thomas, *Biofibres and biocomposites*, Vol. 71, **2008**, pp. 343–364.

[45] M. Andresen, L. S. Johansson, B. S. Tanem, P. Stenius, *Cellulose* **2006**, *13*, 665.

[46] M. A. S. Azizi Samir, F. Alloin, A. Dufresne, *Biomacromolecules* **2005**, *6*, 612.

[47] S. Montanari, M. Roumani, L. Heux, M. R. Vignon, *Macromolecules* **2005**, *38*, 1665.

[48] J. Lee, Y. Deng, *Soft Matter* **2011**, *7*, 6034.

[49] Y. C. Hsieh, H. Yano, M. Nogi, S. J. Eichhorn, *Cellulose* **2008**, *15*, 507.

[50] G. Guhados, W. Wan, J. L. Hutter, *Langmuir* **2005**, *21*, 6642.

[51] F. Svec, *J Sep Sci* **2005**, *28*, 729.

[52] G. Guiochon, *J Chromatogr A* **2007**, *1168*, 100.

[53] O. G. Potter, E. F. Hilder, *J Sep Sci* **2008**, *31*, 1881.

[54] J. Sproß, A. Sinz, *J Sep Sci* **2011**, *34*, 1958.

[55] M. Ishida, Y. Sashiyama, H. Akamatsu, K. Hayashi, K. Nakanishi, G. Hasegawa, *J Solgel Sci Technol* **2022**, *104*, 526.

[56] G. Hasegawa, T. Shimizu, K. Kanamori, A. Maeno, H. Kaji, K. Nakanishi, *Chemistry of Materials* **2017**, *29*, 2122.

[57] T. Zhang, Z. Xu, H. Chi, Y. Zhao, *ACS Appl Polym Mater* **2020**, *2*, 2578.

[58] Z. Yang, T. A. Asoh, H. Uyama, *Bull Chem Soc Jpn* **2019**, *92*, 1453.

[59] A. Namera, A. Nakamoto, T. Saito, S. Miyazaki, *J Sep Sci* **2011**, *34*, 901.

[60] P. Paraskevopoulou, I. Smirnova, T. Athamneh, M. Papastergiou, D. Chriti, G. Mali, T. Čendak, M. Chatzichristidi, G. Raptopoulos, P. Gurikov, *ACS Appl Polym Mater* **2020**, *2*, 1974.

[61] Y. Xin, Q. Xiong, Q. Bai, M. Miyamoto, C. Li, Y. Shen, H. Uyama, *Carbohydr Polym* **2017**, *157*, 429.

[62] Y. Habibi, *Chem Soc Rev* **2014**, *43*, 1519.

[63] C. Qian, T. Higashigaki, T. A. Asoh, H. Uyama, *ACS Appl Mater Interfaces* **2020**, *12*, 27518.

[64] S. Gorgieva, S. Hribernik, *Nanomaterials* **2019**, *9*, 303.

[65] M. P. H. Pedige, T. A. Asoh, Y. I. Hsu, H. Uyama, *Carbohydr Polym* **2022**, *278*, 118907.

[66] Q. Wang, T. A. Asoh, H. Uyama, *RSC Adv* **2018**, *8*, 12608.

[67] A. Šturcová, G. R. Davies, S. J. Eichhorn, *Biomacromolecules* **2005**, *6*, 1055.

[68] S. Beck-Candanedo, M. Roman, D. G. Gray, *Biomacromolecules* **2005**, *6*, 1048.

[69] A. Gevorkian, S. M. Morozova, S. Kheiri, N. Khuu, H. Chen, E. Young, N. Yan, E. Kumacheva, *Adv Funct Mater* **2021**, *31*, 2010743.

[70] A. Bin Imran, T. Seki, Y. Takeoka, *Polym J* **2010**, *42*, 839.

[71] S. A. Greenberg, T. Alfrey, *J Am Chem Soc* **1954**, *76*, 6280.

[72] Y. Okada, F. Tanaka, *Macromolecules* **2005**, *38*, 4465.

[73] P. Kujawa, F. M. Winnik, *Macromolecules* **2001**, *34*, 4130.

Chapter 1

Stiffness-Changing Materials with Shape Stability Based on Cellulose Monolith and Poly(stearyl methacrylate)

1-1. Introduction

Stiffness-changing materials (SCMs) are smart materials whose stiffness can be altered in response to environmental stimuli, such as temperature,[1–3] light,[4] pH,[5] and hydration.[6–8] SCMs have found widespread use in industrial applications, for example, as robotics components,[9] vibration damping devices,[10] and biomimetic materials.[11] For practical implementation, it is crucial that SCMs have the requisite mechanical properties, a high degree of adaptability, a stable and lightweight structure, and reversible cycling durability. Designing a material with changeable stiffness requires building blocks capable of binary synergism: a responsive domain and a supporting network.[12,13] The stiffness of the responsive component must be adjustable in response to external stimuli to activate switchable interaction or conformational changes, such as cross-linking by dynamic covalent bonds or noncovalent interactions,[1,2,5,6,8,14] crystallization-melting or glass transition of thermoplastics,[15–18] supercooling materials,[19–21] and polymer vitrification.[22] These mechanisms have the potential to induce different configurations of materials and consequently alter their mechanical properties. Failure occurs because the responsive unit alone does not have sufficient rigidity to sustain the architecture such that it remains robust during changes in response to stimuli. To overcome this obstacle, a reinforcing framework is essential as an effective component, including a robust polymeric structure,[2,23] owing to its ability to form combinations with responsive units to provide structural stability for practical use.

Highly porous monolithic materials have fascinated researchers owing to their interesting properties, such as their light weight, large surface area, and low density, which are derived from their hierarchical pore and through-pore structures.[24,25] Among them, monoliths composed of organic polymers display great flexibility and toughness with dimensional stability compared with those composed of inorganic raw materials with brittleness.[26] In addition, compared to networks composed of soft materials such as hydrogels and elastomers, organic monoliths have relatively high rigidity and dimensional stability. Therefore, polymeric monoliths are expected to be useful as supports for materials with variable stiffness. Cellulose monoliths (CMs), environmentally friendly materials with a hierarchically porous structure, were developed by a facile thermally

induced phase separation technique using cellulose acetate as a starting material. These CMs also demonstrate exceptional chemical and physical stability and robustness against temperature variations. In addition, the hydroxyl groups on the cellulose chain facilitate surface modification. Also, the skeletal backbone of CM composed of amorphous cellulose has high porosity, allowing great permeability of substances into the backbone as well as pores of CM. Furthermore, CM exhibits formability into a variety of desirable shapes because the precursor of the monoliths is a polymer solution of cellulose acetate. These favorable properties have led to the application of the CM in catalysis,[27] ion exchange,[28] adsorption,[29] and chromatography.[30] Moreover, because of its porous nature, the CM can absorb solvents, which enables effective functionalization not only on the surface but also on the backbone in the interior. Therefore, the functionalized responsive components of SCMs in the CM are expected to be densely packed, thereby conferring excellent mechanical robustness. Apart from this, the good swellability and flexibility of CM in water enables materials with variable stiffness to be accommodated and allows the CM to function under aqueous conditions, including in biological environments.[31]

Poly(stearyl methacrylate) (PSMA) is a semicrystalline comb-type polymer with a long aliphatic pendant group, and its side chains tend to form stacked crystals with an ordered structure despite the amorphous main chain.[32–34] Because of the closely packed side chains, PSMA demonstrates a dramatic phase transition between the crystalline and melted states in response to cooling and heating, respectively. PSMA has considerable rigidity below the melting temperature owing to the crystallization of the polymer. On the other hand, above the melting temperature, the alkyl chains become amorphous, and the polymer becomes flexible as a result of undergoing a phase change. PSMA is used in a wide range of temperature-triggered applications, such as sensors,[35] optical modulation in display technology,[36,37] shape-deformable gels,[38–40] and self-assembly from amphiphilic polymers;[41,42] thus, the polymer is also a promising candidate for a responsive unit of the SCM. Owing to the sharp phase change and reversibility in response to temperature, the stiffness changes rapidly within a short response time, and these changes are repeatable for multiple operating cycles.[33] These characteristics make these polymers highly suitable for use as dynamically operating responsive units in materials of which the stiffness changes over time.[43–47]

In this study, thermoresponsive PSMA was composited with CM to develop SCMs with high structural stability. CM, as the skeletal supporting network, was fabricated and modified with an

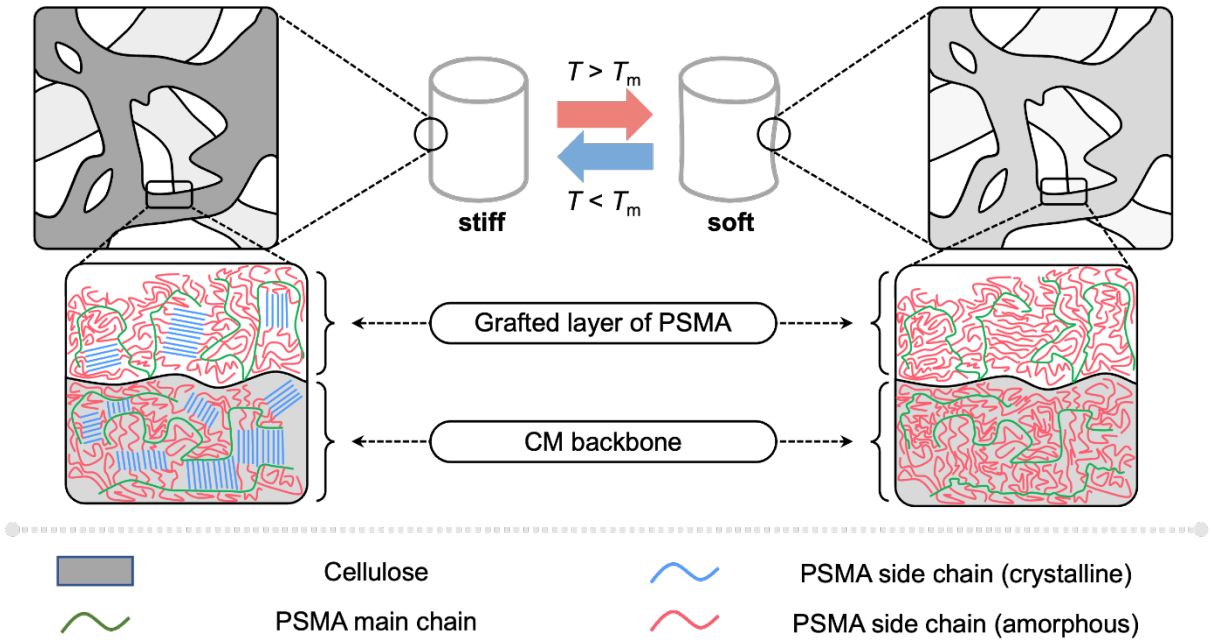

Figure 1-1. Conceptual illustration of the stiffness-changing monolith.

acryloyl (AC) group. PSMA, as the responsive domain, was incorporated into CM by free-radical polymerization of stearyl methacrylate (SMA) in the presence of AC-modified CM. The PSMA domain contributed its characteristic ability to undergo a stiffness change to the PSMA-modified CM (PSMA-CM). (**Figure 1-1**) In addition, the cellulose domain of CM provided the reinforcing effect to sustain both the structural stability of the material and the soft nature of PSMA as the responsive domain, which are generally in a trade-off relationship. The mechanical properties of PSMA-CM were analyzed to determine, for example, the effect of the changes in the temperature and polarity of the solvents on the stiffness. Moreover, the shape recoverability and the repeatability of the stiffness change were investigated using a series of mechanical tests at various temperatures.

1-2. Experimental Section

Materials

CA (average M_n ~50,000), 1-hexanol, and 2,2'-azobis(isobutyronitrile) (AIBN) were purchased from Sigma-Aldrich (USA). Triethylamine (TEA) and *N*,*N*-dimethylformamide (DMF) were purchased from Nacalai Tesque Inc. (Japan). Acryloyl chloride and sodium hydroxide were purchased from Fujifilm Wako Pure Chemical Corporation (Osaka, Japan). Stearyl methacrylate

(SMA) was purchased from Tokyo Chemical Industry Co., Ltd. (Japan). All chemicals were used as received.

Preparation of Cellulose Monolith

CM was produced using the TIPS technique according to a previous study.[48] Briefly, 3.0 g of CA was added to 10 mL of DMF at 90 °C and stirred until the CA was completely dissolved. Subsequently, 15 mL of 1-hexanol was added dropwise, and the mixture was heated to 90 °C until it became transparent. The obtained solution was molded into cylindrical glass cups (with a diameter of 10 mm) and cooled at 20 °C for 6 h to complete the phase separation. The solvent was exchanged with methanol three times a day for 2 days to obtain the CA monolith (CAM). The CAM was deacetylated in an alkaline medium (0.5 M NaOH in methanol) for 3 h and washed with ethanol for 1 day to obtain the CM. The monolith was dried under a vacuum and stored in a dried state.

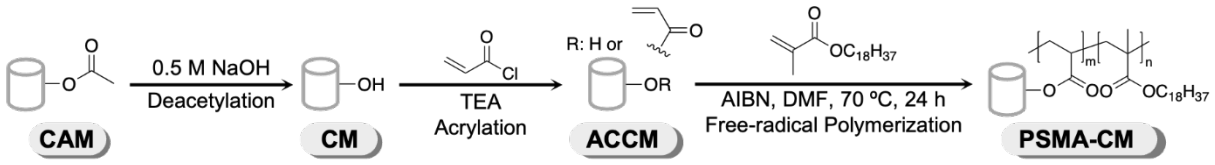

Figure 1-2. Schematic illustration of the preparation of PSMA-CM.

Chemical Modification of Cellulose Monolith with Acryloyl Chloride

The acryloyl group was immobilized onto the surface of CM by the condensation reaction between the hydroxy group of CM and acryloyl chloride. The dried CM (1.9 g, 12 mmol of anhydrous glucose unit) was soaked in DMF (15 mL), whereupon TEA (17.8 g, 0.18 mol) was added to the mixture. Following stirring in an ice bath for 3 h, acryloyl chloride (28.6 mL, 10 equiv toward the hydroxy group of cellulose) was added dropwise with stirring. The reaction was allowed to proceed for 24 h at room temperature. The resulting product was rinsed several times with deionized (DI) water to remove unreacted chemicals and byproducts to obtain acryloyl group-modified CM (ACCM, **Figure 1-2**).

Grafting of Poly(stearyl methacrylate) onto the Cellulose Monolith

PSMA was grafted onto the CM via free-radical polymerization of SMA in the presence of ACCM. The ACCM (2.1 g) was soaked in a solution of SMA (15, 30, and 50 wt% to weight of

ACCM) and AIBN (1.0 mol % of SMA) in DMF (15 mL). The mixture was stirred for 24 h at room temperature and degassed with a vacuum pump for 10 min. Then, the solution was heated at 70 °C for 24 h to induce free radical polymerization. After the reaction, the PSMA-grafted CM (PSMA-CM) was thoroughly washed twice with DMF and consequently DI water prior to characterization. In *x*PSMA-CM, *x* represents the feed weight fraction of the SMA.

Characterization

Scanning electron microscopy (SEM, Hitachi SU3500N, Japan) with an accelerating voltage of 15 kV was used to observe the morphology of the monoliths. The interior part of monoliths was observed using the cross-sectional samples, which were obtained by being cut and gently split. Prior to the observation, the interior surface was sputtered with Au-Pd using a Magnetron Sputter (MSP-1S, Vacuum Device, Japan). Attenuated total reflection Fourier transform infrared (ATR-FTIR) spectra were recorded using a Nicolet iS 5 spectrometer coupled with an iD5 ATR attachment (Thermo Scientific, USA). The melting and recrystallization temperatures were analyzed by differential scanning calorimetry (DSC) (Seiko DSC6220, Japan) at heating and cooling rates of 10 °C min^{-1} and a temperature program in the range from 10 to 50 °C. The enthalpy values of melting and crystallization were calculated from the area under the melting and recrystallization peaks of the DSC thermogram, respectively.

Water Uptake Measurement

The hydrophilicity of the monoliths was evaluated by water uptake measurements. PSMA-CM, which had been previously dried, was submerged in water. After a specified duration, the monoliths were retrieved carefully, the excess water was removed, and the monoliths were weighed. The water uptake (WU) of the monoliths was defined using **eq 1**, where w_h and w_0 are the weights of the swollen and dehydrated monoliths, respectively.

$$\mathrm{WU} = \frac{w_h - w_0}{w_0} \times 100 \quad (1)$$

Compression Test

The specimens for the compression test were fabricated by preparing cylindrical samples (approximately 1 cm in radius and 1 cm in height). The mechanical strength of the monoliths was

assessed using uniaxial compression testing. A universal testing machine (Shimadzu EZ Graph, Japan) was used with a deformation speed of 3.0 mm min^{-1}. The compression test was performed under the following two different conditions: (1) samples were immersed in deionized water and compressed at different temperatures (approximately 20, 40, and 60 °C), and (2) samples were immersed in various solvents to determine the effect of the polarity of the environment. The samples were compressed at room temperature after sufficient solvent conversion. Water, ethanol, acetone, and hexane were used as solvents in the case of a single solvent system. In addition, a solvent mixture of hexane and acetone was used as a binary co-solvent system with volumetric fractions of hexane (φ_h) of 0, 0.2, 0.4, 0.6, 0.8, and 1.0.

Recoverability Measurement

The loading–unloading measurements were performed by conducting the compression test at 3.0 mm min^{-1} using a universal testing machine (Shimadzu Autograph AGS-X L3744, Japan). Samples were immersed in water at various temperatures of approximately 20, 40, and 60 °C and then compressed to compression ratios of 5, 10, 15, 20, 25, and 30%. The unloading procedure proceeded briefly, following the defined compression level in each cycle. The stress–strain curves were recorded during the loading and unloading tests.

Cyclic compression was performed to measure the recoverability of the monoliths. The samples were compressed to 20% and unloaded, at 60 and 20 °C alternately, for 10 cycles. To ensure a uniform environment, the monolith sample was immersed in water at 20 °C for 10 min. The monolith was then subjected to compression to 20%. After compression, the monolith was unloaded and heated to 60 °C for 10 min. Subsequently, the monolith underwent recompression. The process was repeated for 10 cycles. The appearance of the monoliths was observed before and after cyclic compression to define their recoverability.

1-3. Results and Discussion

Characterization of PSMA-CM

PSMA-CM was fabricated by immobilizing PSMA into CM via the polymerization of SMA with the acryloyl

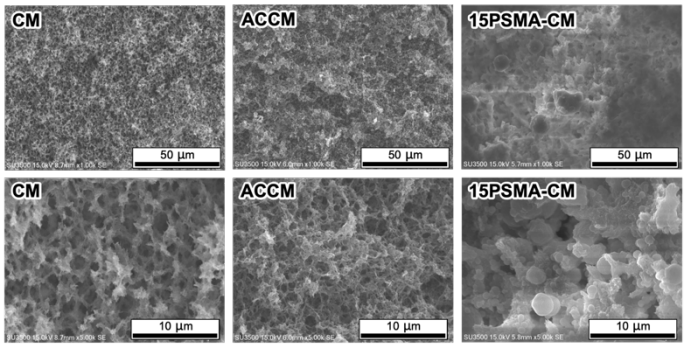

Figure 1-3. SEM images of the porous morphology of CM, ACCM, and 15PSMA-CM.

groups on ACCM (**Figure 1-2**). The morphologies of CM, ACCM, and PSMA-CM were assessed by acquiring SEM images, which are shown in **Figure 1-3**. The CM exhibited a porous structure, and a similar morphology was observed for ACCM after modification with the acryloyl group. In contrast, the morphology of PSMA-CM differed in that the particles had grown onto the skeletal backbone of the monolith, supporting that PSMA was successfully grafted on the surface of CM.

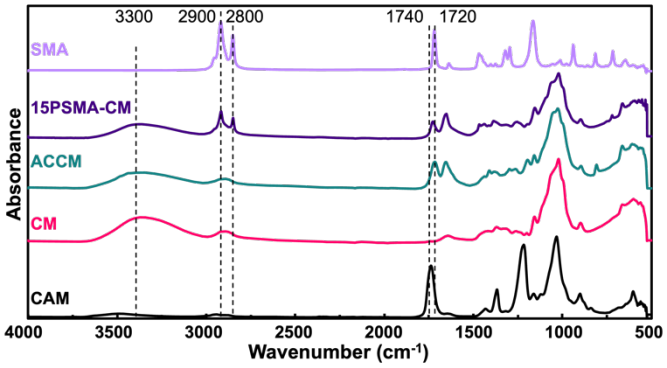

Figure 1-5. FTIR spectra of CAM, CM, ACCM, 15PSMA-CM, and SMA.

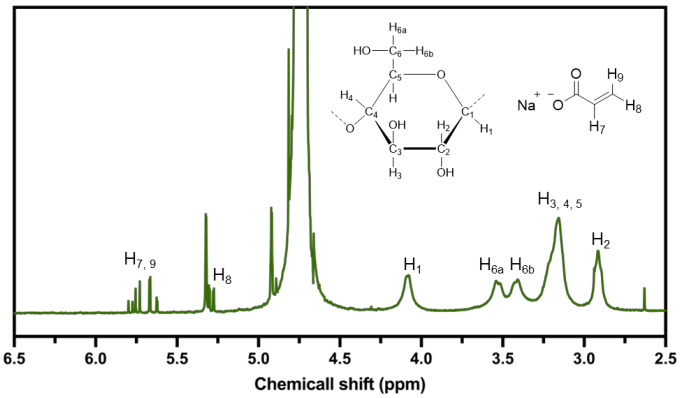

Figure 1-4. ^{1}H NMR spectrum of ACCM in NaOD/urea/D_2O describing the degree of substitution of acryloyl group = 0.09.

FTIR spectra were recorded to characterize the monoliths (**Figure 1-5**). An intense peak, resulting from the C═O stretching vibration, was observed at 1740 cm^{-1} on the spectrum of CAM but disappeared from that of CM, revealing that deacetylation had proceeded. In addition, the CM exhibited a broad peak at 3000-3500 cm^{-1} attributed to the O-H stretching vibration of the hydroxyl groups. The new band at 1720 cm^{-1} on the spectrum of ACCM was related to the C═O stretching vibration, indicating that acryloyl groups were immobilized onto the CM. Additionally, the immobilization of acryloyl group onto CM was also characterized by ^{1}H NMR measurement (**Figure 1-4**). The spectrum of PSMA-CM presented absorption bands centered at 2800 cm^{-1}, which were attributed to the C–H stretching vibration and identified to correspond to bands in the similar region on the spectrum of SMA. On the basis of

Table 1-1. The composition of grafted PSMA in PSMA-CM.

Sample	feed amount of SMA (wt%)	grafted amount of PSMA (wt%)
15PSMA-CM	15	14.24 ± 1.57
30PSMA-CM	30	28.22 ± 0.40
50PSMA-CM	50	45.22 ± 1.27

these results, PSMA was concluded to have been incorporated into the CM. The PSMA-CM samples were analyzed using DSC measurements, which revealed an endothermic peak at approximately 38 °C during heating and an exothermic peak at approximately 22 °C during cooling, as shown in **Figure 1-6a and b**. These two peaks were attributed to the melting and recrystallization of the alkyl side chains in PSMA, respectively. The values of the enthalpy of melting and recrystallization, calculated from the area under these peaks in the DSC thermograms, are compared in **Figure 1-6c**. These enthalpy values increased as the feed weight ratio of SMA increased. This demonstrates that the crystallizable segment increased as the amount of PSMA increased. Additionally, the enthalpy values for the melting and crystallization of pure PSMA were 76 and −57 J g^{-1}, respectively, exhibiting that the enthalpy values of each PSMA-CM were within the appropriate range (black spectra in **Figure 1-6a and b**). Furthermore, the appearance of melting and recrystallization peaks indicated that the crystallization/melting transition of PSMA was maintained even after being incorporated into the monolith structure. On the other hand, as the amount of SMA in the feed increased, the temperature at which the crystallization/melting transition occurred shifted toward lower temperatures. This indicates that the temperature of the transition and the temperature at which the stiffness of the monoliths changes depend on the amount of SMA in the feed because the PSMA content immobilized on the monolith is closely related to that of free PSMA.[49]

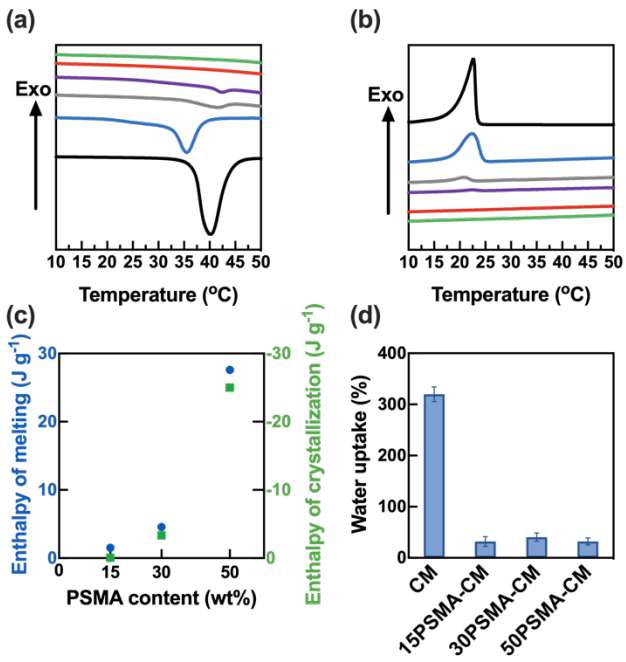

Figure 1-6. DSC (a) heating and (b) cooling thermograms of (green) CM, (red) ACCM, (violet) 15PSMA-CM, (gray) 30PSMA-CM, (blue) 50PSMA-CM, and (black) free PSMA. (c) Enthalpy of melting and recrystallization of PSMA-CM samples. (d) Water uptake measurements of CM and PSMA-CM.

To further confirm the successful immobilization of PSMA onto CM, the amount of incorporated PSMA in PSMA-CM was determined via gravimetric analysis (**Table 1-1**). The feed

weight fraction of SMA was closely similar to the amount of grafted PSMA. This result indicated that the amount of PSMA in CM can be controlled by the feed amount of SMA.

In addition, the numerous hydrophilic hydroxy groups of CM were responsible for the high water uptake ratio of this material. In contrast, the PSMA-CM displayed a low uptake ratio (**Figure 1-6d**). This indicates that PSMA was effectively introduced into the monolith. Because the immobilized PSMA has a long aliphatic pendant group, the monolith was highly hydrophobic owing to the concealed side chain. The monolith with varying amounts of PSMA had a roughly similar water uptake. All the results indicated that PSMA had been successfully incorporated into the CM, and the modified PSMA exhibited the properties of PSMA.

Temperature-Dependent Mechanical Properties of PSMA-CM

A comparison of the mechanical properties of CM and PSMA-CM at different temperatures is shown in **Figure 1-7**. The compression of CM to 50% at 20 °C resulted in compressive stress of approximately 0.2 MPa, and this remained unchanged even when the temperature was raised to 60 °C. In contrast, at 50% compression, the increase in the compressive stress of 30PSMA-CM at 20 °C (approx. 0.6 MPa) was comparable to that of CM at this temperature and compression, but the compressive stress decreased when the temperature was increased to 40 °C, near the transition

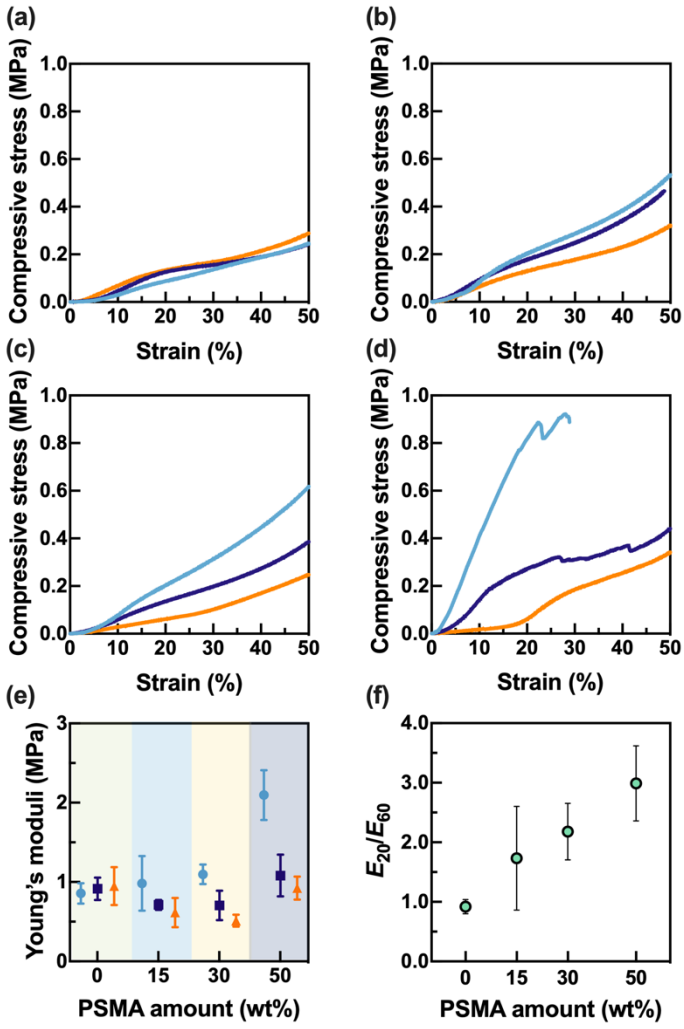

Figure 1-7. Compressive stress-strain curve of (a) CM, (b) 15PSMA-CM, (c) 30PSMA-CM, and (d) 50PSMA-CM at temperature of (light blue) 20, (dark blue) 40, and (orange) 60 °C and (e) Comparison of Young's moduli and grafted PSMA amount under varying temperatures. (f) Ratio of Young's moduli of PSMA-CM under 20 °C (E_{20}) to 60 °C (E_{60})

temperature. The compressive stress of 30PSMA-CM was diminished, compared to that of CM at 60 °C (around 0.2 MPa at 50% compression). 15PSMA-CM similarly demonstrated a decline in compressive strength with increasing environmental temperature, although, at low temperatures, its compressive strength was less than that of 30PSMA-CM (**Figure 1-7c**). In comparison, 50PSMA-CM, upon compression at 20 °C, experienced an increase in compressive strength of 0.9 MPa, but the sample disintegrated at approximately 30% compression. In addition, the compressive stress of this sample was lowered considerably from the initial level of compression when the temperature exceeded 40 °C (**Figure 1-7d**). These results revealed that an increase in the temperature was accompanied by a loss in compressive strength of PSMA-CM. In particular, the amount of PSMA influences the difference in stress between temperatures below and above the transition point. This is attributed to the ordered packing of the PSMA side chain as a rigid unit in the monolith at 20 °C. Below the melting temperature, PSMA-CM is subjected to higher stress and improved mechanical properties. At temperatures above the melting point, the side chain becomes relaxed, and the chain is unpacked, leading to lower stress.

To acquire a comprehensive understanding of the temperature-dependent mechanical properties, the Young's moduli of PSMA-CM and CM were compared (**Figure 1-7e**). Even when the temperature was raised beyond the transition temperature, the Young's modulus of the CM did not change significantly. This confirmed that the CM did not undergo a significant change in thermosensitive behavior. On the other hand, the PSMA-CM samples displayed a shift in their Young's moduli as a function of temperature, revealing that the sample could adapt to changes in temperature. At 20 °C, the Young's modulus of 15PSMA-CM was nearly equivalent to that of CM (approximately 1 MPa), and this value increased to 2 MPa with increasing PSMA content (30PSMA-CM and 50PSMA-CM). This is because, below the transition temperature, the number of crystalline units in the monolith increased owing to the close packing of aliphatic chains, which in turn contributed to greater stiffness. The Young's modulus of 15PSMA-CM was smaller at 40 °C than at 20 °C. This was due to the decrease in the crystallinity and rigidity of PSMA because of the loosening of the aliphatic side chains. The Young's moduli of the PSMA-CM samples declined at 60 °C, which is considerably higher than the transition temperature. This was mainly because of the lower crystallinity at higher temperatures as a result of the relaxation of aliphatic side chains. Importantly, PSMA-CM had a lower Young's modulus than the unmodified CM at 60 °C. This is probably because PSMA was not only attached to the surface of the porous skeletal

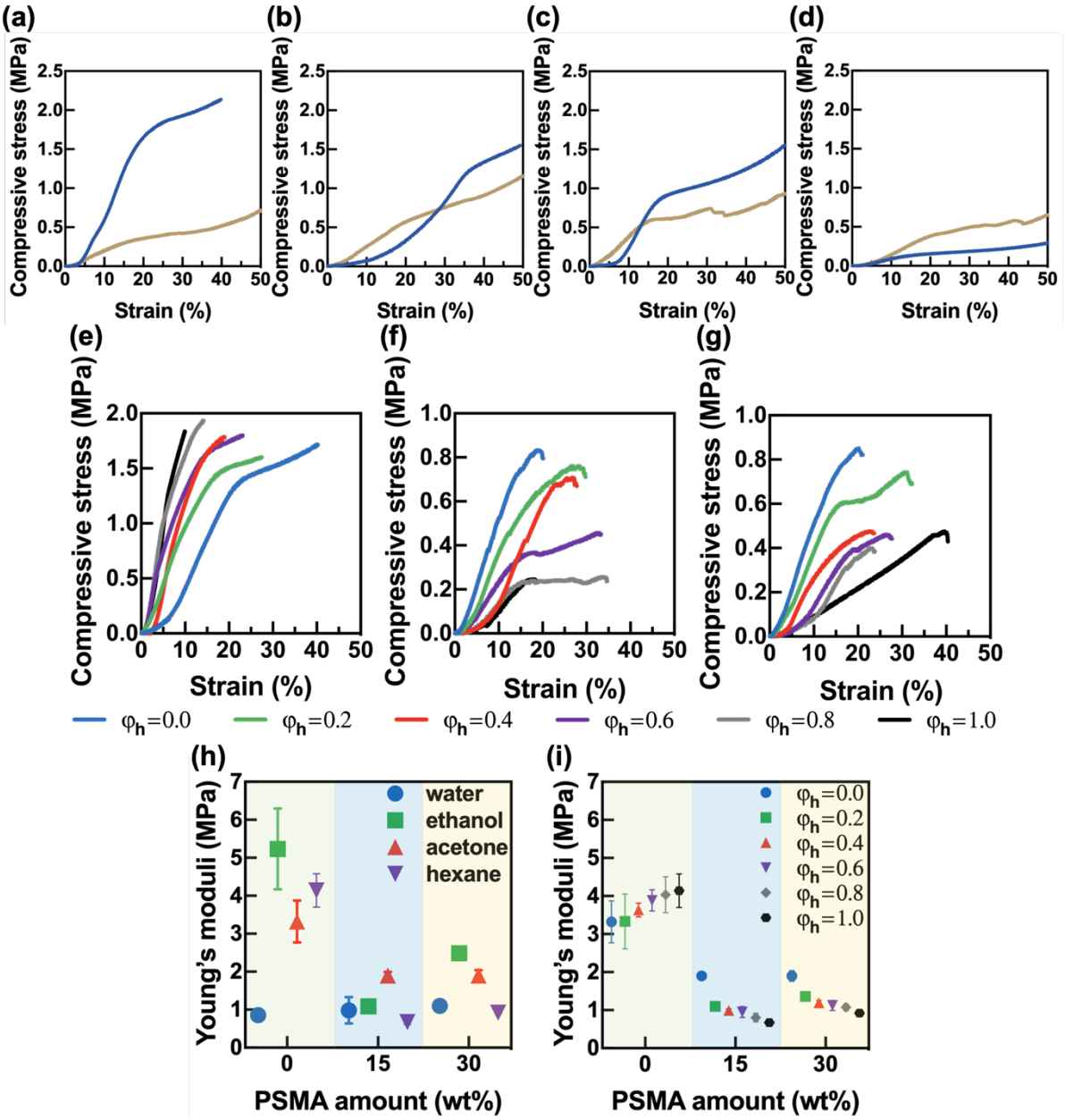

Figure 1-8. Compressive stress-strain curves of CM and 15PSMA-CM under common (a) water, (b) ethanol, (c) acetone, and (d) hexane immersion. Compressive stress-strain curves of (e) CM, (f) 15PSMA-CM, and (g) 30PSMA-CM under varying volume fraction of acetone:hexane cosolvent system. Comparison of Young's moduli and amount of grafted PSMA immersed in various (h) common solvents and (i) volume fractions of the acetone/hexane co-solvent system.

structure of CM but also incorporated into the interior of the CM skeleton, thereby lowering the degree of hydrogen bonding among the cellulose chains of CM. This clearly reflects the changes in the stiffness of PSMA as the responsive component of PSMA-CM materials at both high and

low temperatures and indicates that the mechanical properties of PSMA-CM are dominated by the nature of PSMA at different temperatures. In other words, CM acts as a stable supporting material and does not disrupt the ability of PSMA-CM to undergo stiffness changes, particularly when PSMA is in the soft state. The properties associated with the stiffness change of the PSMA-CM were additionally evaluated by calculating the ratio of the Young's moduli at 20 and 60 °C (E_{20}/E_{60}) (**Figure 1-7f**). The value of E_{20}/E_{60} of CM was close to 1, revealing that the Young's modulus was temperature independent. In contrast, the value of E_{20}/E_{60} of PSMA-CM increased linearly up to a value of 3 in relation to the amount of grafted PSMA. This variation resulted from the difference between the stiffer nature of PSMA-CM as the amount of PSMA increased at low temperatures and the significantly softer nature of PSMA-CM at high temperatures. 15PSMA-CM exhibited stiffness-changing behavior even though the amount of incorporated PSMA was relatively low, whereas the value of E_{20}/E_{60} was also comparatively small. These results indicate that a dynamic range of stiffness switching existed for PSMA-CM in response to temperature, which is consistent with the behavior of PSMA at the crystallization/melting phase transition (**Figure 1-1**).

Influence of the Solvent Polarity on the Mechanical Properties of PSMA-CM

PSMA, with its long aliphatic side chains, is reported to preferentially dissolve in nonpolar organic solvents and oils.[34] The difference in the compatibility of PSMA-CM with different solvent environments would therefore be expected to affect the stiffness. Compression tests were conducted to examine the effect of solvent polarity on PSMA-CM compared to that on CM in the common solvents, water, acetone, ethanol, and hexane (**Figure 1-8a-d and h**). CM exhibited a low Young's modulus in water owing to the high swellability of cellulose in water. However, the Young's modulus of CM in nonaqueous solvents was remarkably higher than that in water owing to the low compatibility in these solvents. The swellability of cellulose in ethanol and acetone as polar solvents is lower than that in water, and the swellability in hexane is expected to be the lowest among these solvents owing to the significantly poor swellability of cellulose in nonpolar solvents.[50–52] The Young's moduli of CM in these solvents reflected these trends well. On the other hand, PSMA-CM displayed a lower Young's modulus in the organic solvents compared with CM. This indicates that PSMA-CM absorbed these organic solvents within the domain in which PSMA was incorporated. Interestingly, the mechanical strength of PSMA-CM was not derived

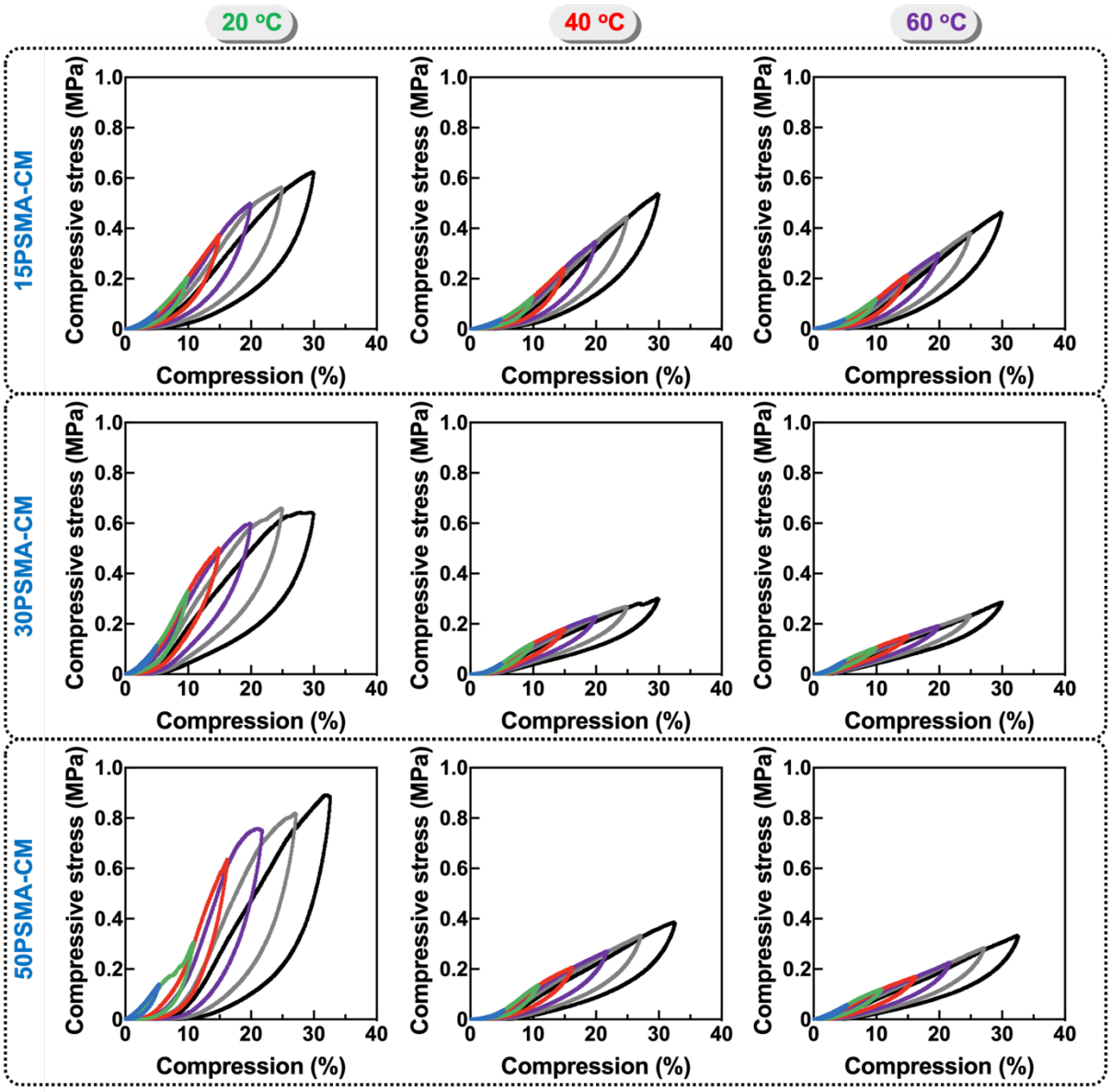

Figure 1-9. Sequential cyclic loading–unloading curves of 15PSMA-CM, 30PSMA-CM, and 50PSMA-CM under different temperatures. Blue, green, red, purple, gray, and black lines represent the cycle at 5, 10, 15, 20, 25, and 30% compression, respectively.

from the cellulose domain to any notable extent, particularly in organic solvents. This result supports that PSMA is the main component in the skeletal network of monoliths, as previously mentioned. On the basis of these results, it was demonstrated that the changeable stiffness of PSMA-CM correlates with the compatibility of PSMA with solvents.

The effect of the polarity on the stiffness was investigated by using acetone and hexane as co-solvents in various proportions as the immersion solvent for a gradual change in polarity (**Figure**

1-8e-g and i). The stiffness of both CM and PSMA-CM shifted gradually as the polarity of the co-solvent system gradually changed. The Young's modulus of CM increased gradually with increasing φ_h. This is because the compatibility of CM with the co-solvents decreases at higher ratios of nonpolar solvents. In contrast, PSMA-CM demonstrated the opposite trend; the PSMA in hexane than in acetone owing to the similar structure of the nonpolar long aliphatic chain of PSMA and hexane. Moreover, the properties of the PSMA domain dominated the stiffening–softening

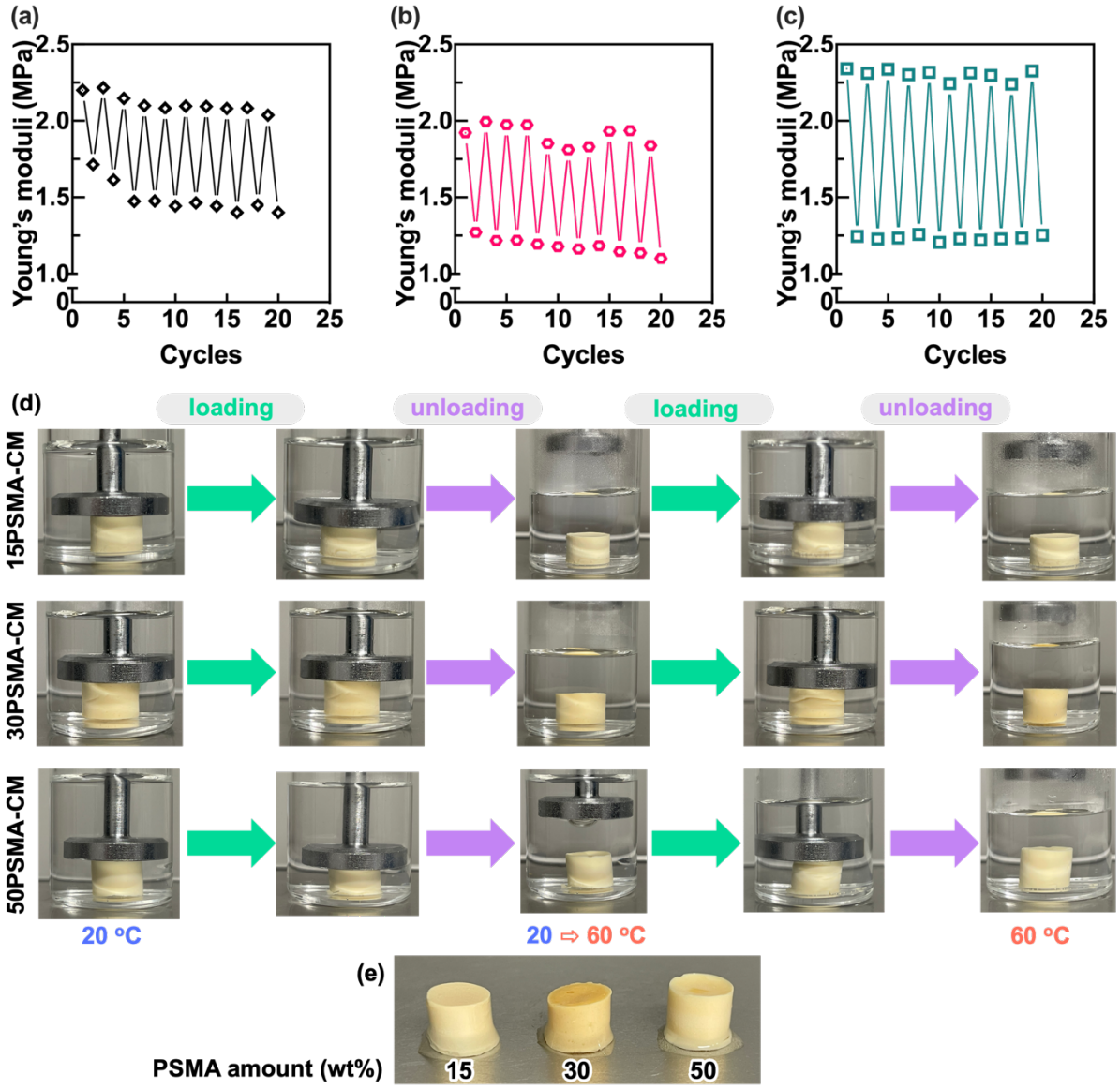

Figure 1-10. Cyclic compression test of (a) 15PSMA-CM, (b) 30PSMA-CM, and (c) 50PSMA-CM during a programmed change in temperature between 20 and 60 °C and photographic images of PSMA-CM (d) during a heating–cooling cycle and (e) after 10 cycles of cyclic compression.

effect of PSMA-CM, as in the case of the temperature response. These results strongly support that PSMA was incorporated into the interior of CM on the skeletal backbone, leading to the suppression of the expression of properties derived from the nature of CM. The reliance of PSMA-CM on the characteristics of PSMA enables PSMA-CM to exhibit variable stiffness in response to solvent polarity.

Recoverability of PSMA-CM

Continuous loading–unloading tests were performed to measure the recoverability of the monolith (**Figure 1-9**). At 40 and 60 °C, each loading curve of PSMA-CM overlapped with the previous ones, although the compression loading–unloading curves presented evidence of considerable hysteresis for each cyclic compression. This result indicates that, in the soft state, PSMA-CM has the potential to quickly recover to its original form. Moreover, even in the stiff state at 20 °C, 15PSMA-CM and 30PSMA-CM exhibited good recoverability up to 20% compression. In contrast, in the case of 50PSMA-CM at 20 °C, the stress of each loading cycle decreased compared with that of the preceding cycle for compressive stress in excess of 10%, revealing relatively low recoverability. This is mainly because 50PSMA-CM with the excess amount of PSMA fractured at a high compression ratio due to the highly stiff nature at 20 °C. These results revealed that 15PSMA-CM and 30PSMA-CM demonstrated great recoverability in both the stiff and soft states.

The recoverable properties of PSMA-CM were additionally assessed by repeated compression testing at 20 and 60 °C. A monolithic sample was periodically compressed during the heating–cooling cycle. With successive cycles, the PSMA-CM demonstrated great repeatability in terms of the change in temperature and compressibility, and the Young's moduli diminished by approximately 13–18% overall for all the PSMA-CM samples, attesting to their thermoresponsive behavior (**Figure 1-10a–c**). The PSMA-CM specimens were visually inspected before and after they were compressed 10 times (**Figure 1-10d and e**), but no noticeable failure in its ability to modulate stiffness was detected. In fact, the PSMA-CM specimens retained their size and shape, indicating that PSMA-CM can recover its original shape after successive cycles of compression.

1-4. Conclusions

In this study, the author developed a monolith comprising a combination of CM and PSMA, of which the stiffness is altered in response to external stimuli. PSMA-CM underwent temperature- and polarity-dependent stiffness changes. Below the melting temperature, PSMA-CM exhibited mechanical stiffness but transformed to a soft state as the temperature rose beyond this temperature. In addition, the mechanical properties of the monolith were directly affected by the polarity of the surrounding solvents. The stiffness decreased as the ratio of hexane to acetone in the mixture increased, indicating that the aliphatic side chain of PSMA was swollen by immersion in a nonpolar solvent. Interestingly, the stimuli-responsive behavior of PSMA-CM was dominated by the properties of PSMA even though cellulose was composited as a rigid framework in the material. This is owing to the formation of a PSMA–cellulose intermingled structure. Cyclic loading–unloading compression of PSMA-CM demonstrated that the shape, stiffness, and thermoresponsive stiffness-changing behavior were maintained after successive deformation. On the basis of these results, PSMA-CM, as a conceptual model of binary materials composed of a combination of porous materials and responsive polymers, is expected to be a unique stiffness-switching material with prospective application in shape memory polymers, actuators, force sensors, and soft robotics with mechanical stability and tunable flexibility.

1-5. References

[1] J. Wu, B. Wu, J. Xiong, S. Sun, P. Wu, *Angew Chem Int Ed* **2022**, *61*, e2022049.

[2] J. Jian, Y. Xie, S. Gao, Y. Sun, C. Lai, J. Wang, C. Wang, F. Chu, D. Zhang, *Carbohydr Polym* **2022**, *294*, 119760.

[3] K. Sano, N. Igarashi, Y. Ebina, T. Sasaki, T. Hikima, T. Aida, Y. Ishida, *Nat Commun* **2020**, *11*, 6026.

[4] R. S. Stowers, S. C. Allen, L. J. Suggs, K. S. Anseth, *Proc Natl Acad Sci U S A* **2015**, *112*, 1953.

[5] T. M. FitzSimons, E. V. Anslyn, A. M. Rosales, *ACS Polym Au* **2022**, *2*, 129.

[6] F. Gao, Y. Zhang, Y. Li, B. Xu, Z. Cao, W. Liu, *ACS Appl Mater Interfaces* **2016**, *8*, 8956.

[7] J. R. Capadona, K. Shanmuganathan, D. J. Tyler, S. J. Rowan, C. Weder, *Science (1979)* **2008**, *319*, 1370.

[8] J. H. Xu, S. Ye, J. J. Fu, *J Mater Chem A Mater* **2018**, *6*, 24291.

[9] L. Wang, Y. Yang, Y. Chen, C. Majidi, F. Iida, E. Askounis, Q. Pei, *Mater Today* **2018**, *21*, 563.

[10] Q. Yang, G. Li, *Smart Mater Struct* **2014**, *23*, 105032.

[11] M. Rong, H. Liu, M. Scaraggi, Y. Bai, L. Bao, S. Ma, Z. Ma, M. Cai, D. Dini, F. Zhou, *Adv Funct Mater* **2020**, *30*, 2004062.

[12] W. Meesorn, J. O. Zoppe, C. Weder, *Macromol Rapid Commun* **2019**, *40*, 1800910.

[13] Z. Zhao, Y. Liu, K. Zhang, S. Zhuo, R. Fang, J. Zhang, L. Jiang, M. Liu, *Angew Chem* **2017**, *129*, 13649.

[14] C. Qian, T. A. Asoh, H. Uyama, *J Mater Chem B* **2020**, *8*, 2400.

[15] T. Xie, *Nature* **2010**, *464*, 267.

[16] K. Sato, T. Nakajima, T. Hisamatsu, T. Nonoyama, T. Kurokawa, J. P. Gong, *Advanced Materials* **2015**, *27*, 6990.

[17] Y. Liu, L. Wang, H. Lu, Z. Huang, *Mater Chem Front* **2021**, *5*, 8056.

[18] B. Yetiskin, O. Okay, *ACS Appl Polym Mater* **2022**, *4*, 5234.

[19] Y. Xin, T. Gao, J. Xu, J. Zhang, D. Wu, *ACS Appl Mater Interfaces* **2021**, *13*, 50392.

[20] B. S. Chang, R. Tutika, J. Cutinho, S. Oyola-Reynoso, J. Chen, M. D. Bartlett, M. M. Thuo, *Mater Horiz* **2018**, *5*, 416.

[21] F. (Kuo) Yang, A. Cholewinski, L. Yu, G. Rivers, B. Zhao, *Nat Mater* **2019**, *18*, 874.

[22] L. Chen, C. Zhao, J. Huang, J. Zhou, M. Liu, *Nat Commun* **2022**, *13*, 6821.

[23] J. Ruokolainen, R. Mäkinen, M. Torkkeli, T. Mäkelä, R. Serimaa, G. ten Brinke, O. Ikkala, *Science (1979)* **1998**, *280*, 557.

[24] Y. Wang, L. Zhang, T. A. Asoh, H. Uyama, *Mater Adv* **2021**, *2*, 3560.

[25] T. Zhang, Z. Xu, H. Chi, Y. Zhao, *ACS Appl Polym Mater* **2020**, *2*, 2578.

[26] P. Paraskevopoulou, I. Smirnova, T. Athamneh, M. Papastergiou, D. Chriti, G. Mali, T. Čendak, M. Chatzichristidi, G. Raptopoulos, P. Gurikov, *ACS Appl Polym Mater* **2020**, *2*, 1974.

[27] Z. T. Xie, T. A. Asoh, Y. Uetake, H. Sakurai, H. Uyama, *Carbohydr Polym* **2020**, *247*, 116723.

[28] Z. Yang, T. A. Asoh, H. Uyama, *Bull Chem Soc Jpn* **2019**, *92*, 1453.

[29] Q. Bai, Q. Xiong, C. Li, Y. Shen, H. Uyama, *Cellulose* **2017**, *24*, 4275.

[30] L. Zhang, Y. Wang, W. Zhang, Y. I. Hsu, T. A. Asoh, B. Qi, H. Uyama, *ACS Biomater Sci Eng* **2022**, *8*, 2676.

[31] X. Cui, Z. T. Xie, Y. Yamaguchi, T. A. Asoh, H. Uyama, *J Porous Mater* **2021**, *28*, 1411.

[32] G. Sun, M. Zhang, J. He, P. Ni, *J Polym Sci A Polym Chem* **2009**, *47*, 4670.

[33] M. Gao, Y. Meng, C. Shen, Q. Pei, *Adv Mater* **2022**, *34*, 2109798.

[34] A. Darvishi, M. J. Zohuriaan Mehr, G. B. Marandi, K. Kabiri, H. Bouhendi, H. Bakhshi, *Des Monomers Polym* **2013**, *16*, 79.

[35] Y. J. Jin, B. S. Il Kim, W. E. Lee, C. L. Lee, H. Kim, K. H. Song, S. Y. Jang, G. Kwak, *NPG Asia Mater* **2014**, *6*, e137.

[36] Y. Ke, C. Zhou, Y. Zhou, S. Wang, S. H. Chan, Y. Long, *Adv Funct Mater* **2018**, *28*, 1800113.

[37] Y. Xie, F. Guan, Z. Li, Y. Meng, J. Cheng, L. Li, Q. Pei, *Macromol Rapid Commun* **2020**, *41*, 2000290.

[38] H. Jing, L. He, J. Feng, H. Fu, S. Guan, P. Guo, *Soft Matter* **2019**, *15*, 5264.

[39] S. Zhuo, Z. Zhao, Z. Xie, Y. Hao, Y. Xu, T. Zhao, H. Li, E. M. Knubben, L. Wen, L. Jiang, M. Liu, *Sci Adv* **2020**, *6*, 1464.

[40] S. H. Kang, T. Aoki, G. Kwak, *Macromolecules* **2019**, *52*, 7984.

[41] J. Zhou, L. Wang, Q. Yang, Q. Liu, H. Yu, Z. Zhao, *J Phys Chem B* **2007**, *111*, 5573.

[42] Y. J. Jin, J. H. Yoon, T. Sakaguchi, C. L. Lee, G. Kwak, *Adv Funct Mater* **2016**, *26*, 4501.

[43] Y. Yang, Y. Chen, Y. Li, M. Zhiqiang Chen, In *Proceedings - IEEE International Conference on Robotics and Automation*, Institute of Electrical and Electronics Engineers Inc., **2016**, pp. 3871–3877.

[44] G. McKnight, R. Doty, A. Keefe, G. Herrera, C. Henry, *J Intell Mater Syst Struct* **2010**, *21*, 1783.

[45] K. Takashima, H. Kamizono, M. Takenaka, T. Mukai, *ROBOMECH Journal* **2017**, *4*, 17.

[46] Y. Yang, Y. Li, Y. Chen, *Biodes Manuf* **2018**, *1*, 14.

[47] K. Takashima, T. Imazawa, H. Cho, *Journal of Robotics and Mechatronics* **2022**, *34*, 466.

[48] Y. Xin, Q. Xiong, Q. Bai, M. Miyamoto, C. Li, Y. Shen, H. Uyama, *Carbohydr Polym* **2017**, *157*, 429.

[49] S. Li, H. Wang, L. Liu, H. Xu, H. Shi, *Cryst Eng Commun* **2018**, *20*, 7348.

[50] A. J. Stamm, *Ind Eng Chem* **1935**, *27*, 401.

[51] G. I. Mantanis, R. A. Young, R. M. Rowell, *Cellulose* **1995**, *2*, 1.

[52] G. I. Mantanis, R. A. Young, R. M. Rowell, In *Holzforschung*, **1994**, pp. 480–490.

Chapter 2

Switchable Stiffness of Bacterial Cellulose Composite Reinforced with Thermoresponsive Phase-Change Particles

2-1. Introduction

Stimuli-responsive hydrogels are smart materials that can adjust their mechanical properties in response to external stimuli, such as pH,[1–3] electric field,[4,5] light,[6–8] ionic strength,[9,10] and temperature.[11–13] Among them, thermoresponsive hydrogels have drawn considerable attention owing to the ease of tuning their mechanical properties.[14] These materials can be used in a variety of applications, including artificial muscles,[15] soft biomimetic machines,[16] and soft robotic components,[17] owing to their softness, flexibility, and biocompatibility. To produce a stimuli-responsive hydrogel with both a significant response in switchable mechanical behavior and high stability, binary systems, composed of a stable network and responsive domain, are useful and reasonable to construct the hydrogel network structure.[18–24] In other words, the selection of a suitable structural framework and responsive unit, as well as the design of the network structure are critical for the development of stimuli-responsive hydrogels with high stability.

In this study, the author developed a thermoresponsive hydrogel with switchable mechanical strength by incorporating poly(stearyl methacrylate) (PSMA) as a responsive domain into bacterial cellulose (BC) as a supporting hydrogel. (**Figure 2-1**) BC is a natural hydrogel made of entangled ribbon-shaped ultrafine cellulose nanofibers, fascinating researchers owing to the uniqueness derived from pure cellulose.[25,26] Despite high water content, BC exhibits considerable dimensional stability and suitable mechanical strength for performing stimuli-responses.[1] In addition, the hydroxy groups of cellulose in BC allow effective functionalization.[27,28] Thus, BC was chosen as a stable structural framework for the smart hydrogel. By contrast, PSMA was used as a thermoresponsive domain for the material. PSMA demonstrates a clear phase change between the crystalline and melting states in response to cooling and heating owing to the packed structure of the long aliphatic side chain in a comb-shaped polymer.[29–31] The phase change of

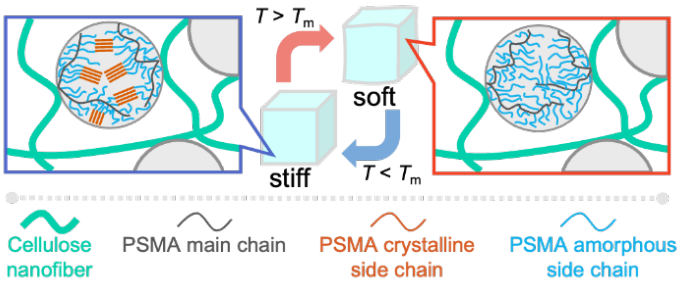

Figure 2-1. Conceptual illustration of thermoresponsive hydrogel with PSMA particle in the BC network.

the PSMA can contribute to the switchable stiffness behavior of smart hydrogels.[32,33] Hence, PSMA particles were incorporated as a reinforcing filler into the BC network to prepare a thermoresponsive composite hydrogel. The mechanical and thermoresponsive properties of the BC hydrogel filled with PSMA particles were investigated to reveal the impact of density and morphologies of PSMA on the responsive behavior.

2-2. Experimental Section

Materials

Nata de Coco seasoned with syrup was purchased from Tengu Kanzume Co. Ltd. (Japan). 2,2'-azobis(isobutyronitrile) (AIBN) was purchased from Sigma-Aldrich (USA). Triethylamine (TEA) and DMF were purchased from Nacalai Tesque Inc. (Japan). Acryloyl chloride was purchased from Fujifilm Wako Pure Chemical Corporation (Japan). SMA was purchased from Tokyo Chemical Industry Co., Ltd. (Japan). All chemicals were used as received.

Chemical Modification of Bacterial Cellulose Hydrogel with Acryloyl Chloride

The acryloyl group was immobilized on the surface of cellulose nanofibers in BC through a condensation reaction between the hydroxy group of cellulose and acryloyl chloride. The purified BC (10.0 g, 6 mmol of anhydrous glucose unit) was soaked in DMF (100 mL), followed by the addition of TEA (12.9 mL, 93 mmol). After 3 h of stirring in an ice bath, acryloyl chloride (15.0 mL, 30 eq. to the number of hydroxy groups in cellulose) was added dropwise while stirring. At 25 °C, the reaction was allowed to proceed for 24 h. The resultant product was rinsed numerous times with deionized (DI) water to remove unreacted chemicals and byproducts and to obtain acryloyl group—modified BC (ACBC, **Figure 2-2**).

Grafting of Poly(stearyl methacrylate) onto Bacterial Cellulose Hydrogel

BC cellulose nanofibers were grafted with PSMA via the free-radical polymerization of SMA in the presence of ACBC. ACBC (10.0 g) was soaked in a solution of SMA (0.97 g to the weight of

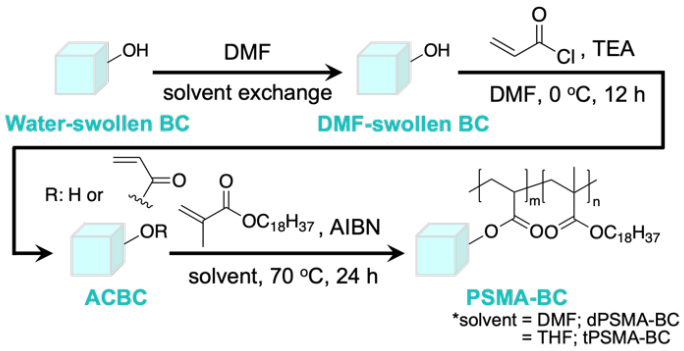

Figure 2-2. Schematic illustration of preparation of PSMA-BC.

ACBC, 0.1 mol L^{-1} in this case) and AIBN (1.0 mol% of SMA) in DMF (18 mL). The mixture was shaken for 24 h at 25 °C and degassed using a vacuum pump for 10 min. To activate free-radical polymerization, the mixture was heated at 60 °C for 24 h. Prior to characterization, the PSMA-BC was washed twice with DMF and then DI water after polymerization. In *xy*PSMA-BC, *x* and *y* represent the abbreviation for solvent used in polymerization, namely t for THF, d for DMF; and the feed concentration of SMA, respectively.

Characterization of Bacterial Cellulose Hydrogel

SEM (Hitachi SU3500N, Japan) with an accelerating voltage of 15 kV was used to observe the morphological structure of the hydrogels. Using ImageJ software, the diameter of around 120 particles was utilized to evaluate the mean and statistical standard deviation of particle sizes. ATR-FTIR spectra were recorded using a Nicolet iS 5 spectrometer coupled with an iD5 ATR attachment (Thermo Scientific, USA). The melting and recrystallization temperatures were analyzed by DSC (SEIKO DSC6220, Japan) at heating and cooling rates of 10 °C min^{-1} and a temperature program in the range of 10-50 °C. The enthalpy of melting and crystallization were calculated from the area under the melting and recrystallization peaks of the DSC thermogram, respectively.

Determination of the Chemical Composition in Bacterial Cellulose Hydrogel

The amount of grafted PSMA was measured by gravimetric analysis. To attain equilibrium, the specimen was soaked in a water bath maintained at 25 °C. The specimen was then retrieved from the water, its surface was gently wiped, and its weight was measured using a balance as water-swollen weight of hydrogel (w_w). In the case of the BC sample, the measured weight is referred to as the pure cellulose weight in hydrogel (w_c). Owing to the complexity of precisely defining this value, the average cellulose weight of hydrogel was approximated. Consequently, the specimen was lyophilized for 48 h, and its weight was measured as the dehydrated weight of hydrogel (w_d). The water content (WC) and grafted PSMA content (WG) of the BC gel were expressed as in **eq 1 and 2**, respectively.

$$\mathrm{WC} = \frac{w_w - w_d}{w_w} \times 100 \quad (1)$$

$$\mathrm{WG} = \frac{w_w - w_d}{w_w} \times 100 \quad (2)$$

Compression test

The mechanical strength of the hydrogels was assessed using uniaxial compression testing. A universal testing machine (Shimadzu EZ Graph, Japan) was used with a deformation speed of 3.0 mm min^{-1}. The compression test was performed under the condition at which the sample was immersed in DI water and compressed at different temperatures (approximately 25 and 50 °C).

2-3. Results and Discussion

Characterization of PSMA-BC

The thermoresponsive hydrogel consisting of PSMA and BC (PSMA-BC) gel was prepared by polymerizing stearyl methacrylate (SMA) in the presence of ACBC (**Figure 2-2**). PSMA was immobilized onto the surface of cellulose fibers in BC by copolymerization. *N*,*N*-dimethylformamide (DMF) and tetrahydrofuran (THF) were used as the solvents in the polymerization, and obtained samples were denoted as dPSMA-BC and tPSMA-BC, respectively. Additionally, the feed concentration of SMA was varied from 0.1 to 0.5 mol L^{-1}. BC hydrogel is basically translucent, whereas after polymerization of SMA, the PSMA-BC gel became opaque (**Figure 2-3**). Additionally, the dimension and shape of PSMA-BC gels were mostly maintained after polymerization. The Fourier-transform infrared (FTIR) spectra revealed that the characteristic signals derived from SMA (C=O and C–H stretching vibrations around 1720 and 2800 cm^{-1}, respectively)

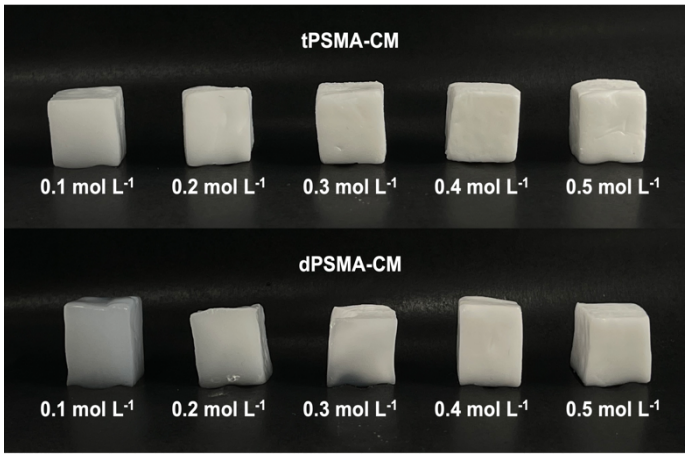

Figure 2-3. Macroscopic illustration of PSMA-BC describing the grafting distribution of PSMA.

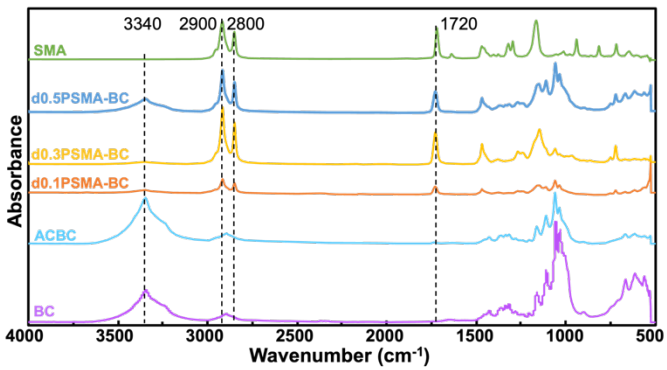

Figure 2-4. ATR-FTIR spectra of BC, ACBC, d0.1PSMA-BC, d0.3PSMA-BC, d0.5PSMA-BC, and SMA.

increased in the spectra of PSMA-BC (**Figure 2-4**). Thus, the modification of PSMA was successfully achieved without distorting the shape of the hydrogel.

The morphological structure of the PSMA-BC gel was observed using scanning electron microscopy (SEM) (**Figure 2-5**). The BC gel exhibited a network structure of cellulose nanofibers, and ACBC gel maintained its network structure after acryloyl group modification (**Figure 2-5a and b**, respectively). By contrast, the PSMA-BC gel exhibited the formation of particles of micrometer-order size in the network of cellulose nanofibers, indicating that PSMA was effectively incorporated into the BC gel (**Figure 2-5c–h**). It was also confirmed that the opacity of the hydrogel was caused by the size of these PSMA particles. Additionally, the opacity of the PSMA-BC gel increased after solvent exchange with water, suggesting that PSMA in BC gel aggregated to form particle structure in water as a poor solvent. The particle size of PSMA in dPSMA-BC gel was about 1 μm, three-fold smaller than that in

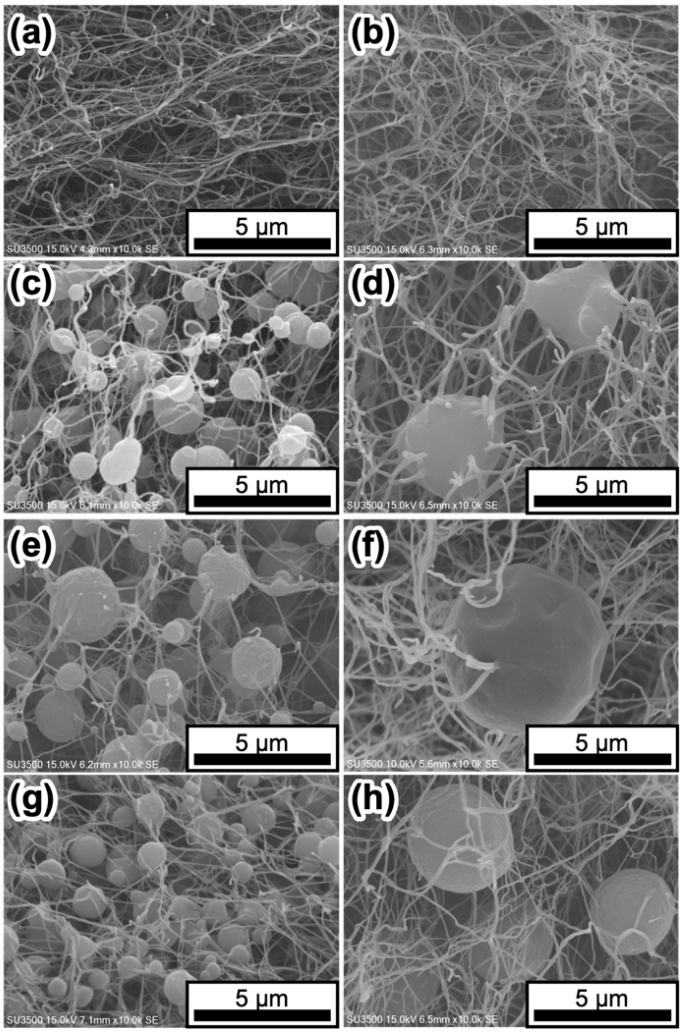

Figure 2-5. SEM images of (a) BC, (b) ACBC, (c,d) 0.1PSMA-BC, (e,f) 0.3PSMA-BC and (g,h) 0.5PSMA-BC gel from dPSMA-BC and tPSMA-BC, respectively.

Table 2-1. Mean diameter and statistical standard deviation of PSMA particle observed in dPSMA-BC and tPSMA-BC.

Feed concentration of SMA (mol L^{-1})	Mean diameter (μm) of PSMA particle in	
	dPSMA-BC	tPSMA-BC
0.1	0.99 ± 0.08	3.51 ± 0.14
0.3	1.30 ± 0.13	3.49 ± 0.08
0.5	1.00 ± 0.04	3.23 ± 0.07

tPSMA-BC gel, and the size remained almost constant under different SMA feed concentrations (**Table 2-1**). Although the grafted PSMA amount was closely similar for both gels, the distribution of particles in the dPSMA-BC gel was relatively homogeneous, compared with that in tPSMA-BC gel, indicating the local distribution of larger particles. The difference in particle size is likely due to the difference in the solubility of PSMA in the solvents. PSMA is more likely to precipitate in DMF than in THF because of the higher polarity of DMF. Therefore, using DMF, the precipitation occurred in the early stage of polymerization to form smaller particles in the BC gel. Furthermore, especially in the case of dPSMA-BC gel as the feed amount of SMA increased, the density of the PSMA particles in the BC network increased (**Figure 2-5c, e, and g**).

Differential scanning calorimetry (DSC) analysis of a lyophilized PSMA-BC sample showed a sharp endothermic peak at about 38 °C during heating owing to the melting of the aliphatic crystalline region and a sharp exothermic peak at about 25 °C while cooling, denoting the recrystallization (**Figure 2-6a-d**). With an increase in feed concentration of SMA, the endothermic and exothermic peaks were shifted to higher and lower temperatures, respectively. Moreover, the enthalpy value of melting and crystallization increased as the feed concentration of SMA increased (**Figure 2-6e and f**). This indicates that the increase in feed concentration of SMA resulted in an increase in not only the amount of PSMA itself but also the crystallizable segment of PSMA synergistically.[34] Furthermore, the dPSMA-BC gel expressed a higher enthalpic value than tPSMA-BC gel with a feed concentration of SMA above 0.3 mol

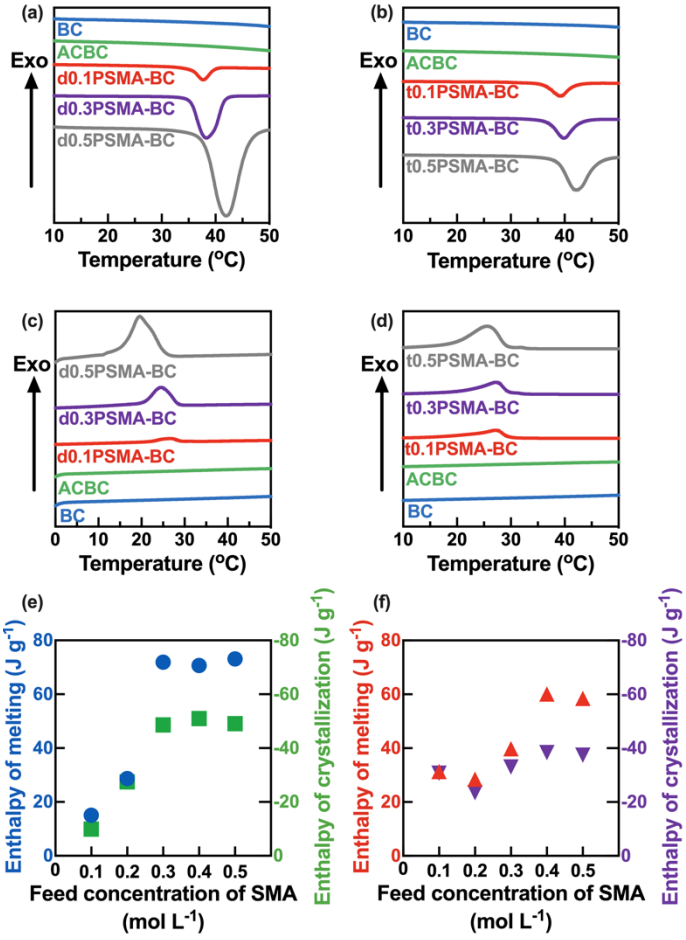

Figure 2-6. DSC thermogram of (a,b) heating and (c,d) cooling processes, and (e,f) enthalpy of melting and crystallization of dPSMA-BC and tPSMA-BC gels, respectively with various amount of feed SMA.

L^{-1}. This also suggests that the crystallizable segment of PSMA in dPSMA-BC gel was greater than that in tPSMA-BC gel.

Subsequently, the actual amount of grafted PSMA and water inside the gels was measured by gravimetric analysis (**Figure 2-7**). With increasing feed amount of SMA in both PSMA-BC gels, the amount of grafted PSMA increased as well as the water content reduced.

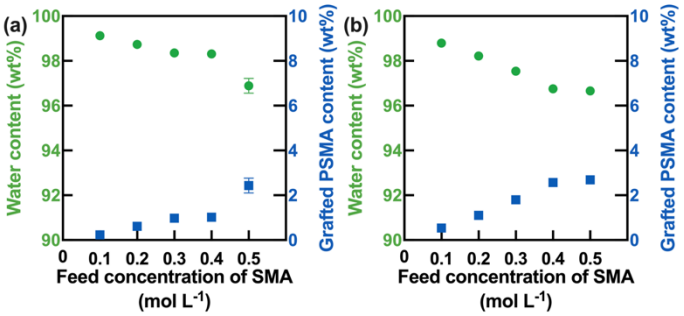

Figure 2-7. Water content and grafted PSMA amount of (a) dPSMA-BC and (b) tPSMA-BC gel prepared by varying the SMA concentration in feed.

Mechanical properties of PSMA-BC

The mechanical strength of BC and PSMA-BC gels was evaluated by compression testing (**Figure 2-8 and 9**). At 25 °C, BC gel had a mechanical strength of 4 kPa at 60% compression, whereas the mechanical strength of d0.4PSMA-BC gel increased as the amount of PSMA increased, reaching a strength of 70 kPa at 60% compression for PSMA-BC gel (**Figure 2-8d and e**). These results indicate that the stiffness of the hydrogel increased by incorporating the PSMA particles in the BC network. Furthermore, when the temperature was elevated to 50 °C, the mechanical strength of BC gel was 3 kPa, which was close to that at 25 °C. However, the stress of d0.4PSMA-BC gel at 50 °C and 60%

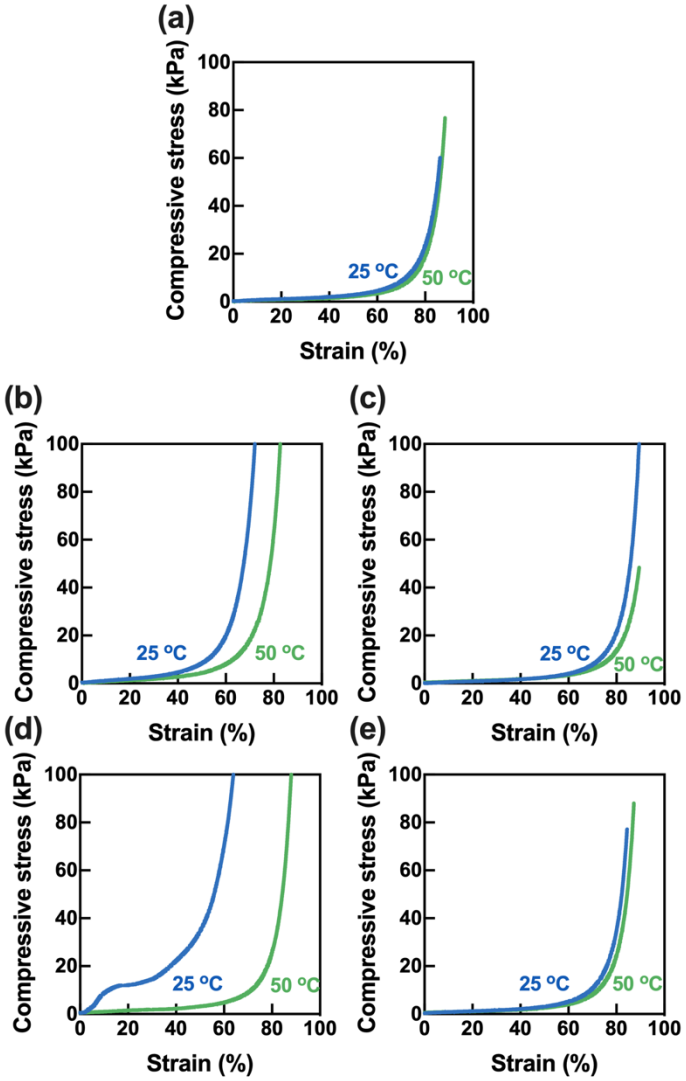

Figure 2-8. Compressive stress-strain curve of (a) BC, (b) d0.3PSMA-BC, (c) t0.3PSMA-BC, (d) d0.4PSMA-BC and (e) t0.4PSMA-BC gels at different temperature.

compression was significantly decreased to 5 kPa. The variation in mechanical strength was apparent with rising SMA feed concentration. These results indicate that the PSMA particles exhibited thermoresponsive mechanical behavior because the packed aliphatic side chain relaxed at elevated temperature.

To further investigate the responsiveness of PSMA-BC gel, Young's moduli at 25 and 50 °C were compared, as shown in **Figure 2-9a and b**. The ratio of Young's moduli under different temperatures (E_{25}/E_{50}) is shown in **Figure 2-9c and d**. In the dPSMA-BC gel, a reduction in Young's modulus was clearly observed with an increase in temperature from 25 to 50 °C, and the gap between Young's moduli at 25 and 50 °C increased with an increasing amount of feed SMA (**Figure 2-9a**). Interestingly, at 50 °C, the dPSMA-BC gel displayed a similar Young's modulus regardless of the amount of PSMA; furthermore, the values of E_{25}/E_{50} were close to 2 at SMA feed concentration below 0.3 mol L^{-1}, whereas the values increased to approximately 8 at a feed concentration above 0.3 mol L^{-1} (**Figure 2-9b**). These results indicate that increasing the amount of PSMA particles drastically improved the mechanical strength of PSMA-BC gel in a stiff state of PSMA at 20 °C because the crystalline PSMA particles acted as stiff reinforcing filler in the PSMA-BC gel. Moreover, the PSMA-BC gel became significantly softened in the soft state of PSMA at 50 °C because the molten PSMA was ineffective as reinforcing particles in their soft state. By contrast, the tPSMA-BC gel exhibited no significant change in Young's modulus and the value of E_{25}/E_{50} with an increase in the amount of PSMA in BC gel, even though the amount of PSMA was similar to that in the dPSMA-BC gel, based on the results of DSC analysis (**Figure 2-9b and d**). This result suggests that the larger and aggregated particles of PSMA in tPSMA-BC gel failed to display a remarkable reinforcing effect for the composite materials. Therefore, the relatively homogeneous distribution

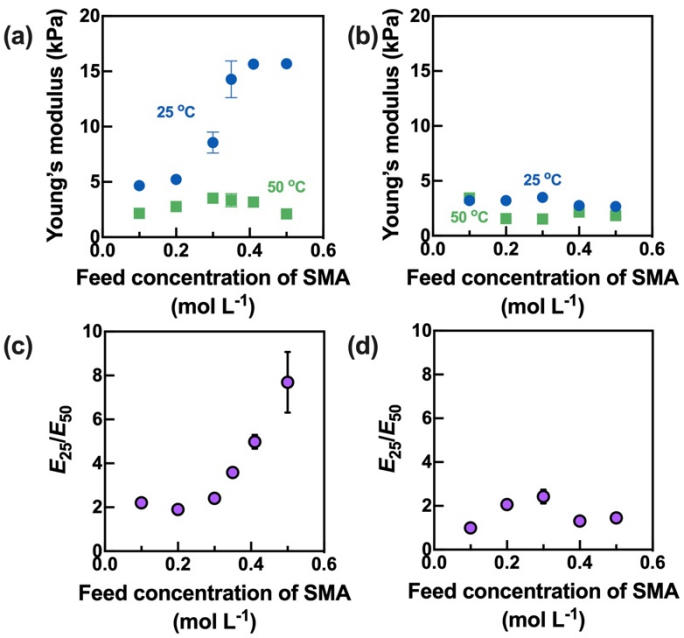

Figure 2-9. (a,b) Comparison of Young's modulus and feed SMA amount under varying temperature and (c,d) ratio of Young's moduli of hydrogels under 25 °C (E_{25}) to 50 °C (E_{50}), prepared from DMF and THF, respectively.

of small PSMA particles in the network of the PSMA-BC gel significantly contributed to the switchable stiffness of the materials in response to temperature.

2-4. Conclusions

In conclusion, a stimuli-responsive hydrogel was effectively developed using BC as a supporting hydrogel network and PSMA as a thermoresponsive domain. In this study, the author proposed the incorporation of PSMA particles into a hydrogel network as a valuable method for enhancing thermoresponsiveness because the particles served as effective reinforcing filler in the materials in a stiff state, while providing less effect on the mechanical strength of the supporting network in a soft state. Furthermore, the density and distribution of PSMA particles influence the responsiveness, and they were controlled with preparation conditions such as solvents and feed concentration of SMA. Additionally, the responsiveness of PSMA-BC gel was tunable by simply tailoring the amount of PSMA, and an increase in the amount of grafted PSMA led to a broadened gap between the stiff and soft states of the final product. The results of this study will promote the industrial usefulness of hydrogels as artificial muscles and soft robotic components.

2-5. References

[1] M. P. H. Pedige, T. A. Asoh, Y. I. Hsu, H. Uyama, *Carbohydr Polym* **2022**, *278*, 118907.

[2] X. Peng, Q. Peng, M. Wu, W. Wang, Y. Gao, X. Liu, Y. Sun, D. Yang, Q. Peng, T. Wang, X. Z. Chen, J. Liu, H. Zhang, H. Zeng, *ACS Appl Mater Interfaces* **2022**, *15*, 19560.

[3] M. Wu, J. Chen, W. Huang, B. Yan, Q. Peng, J. Liu, L. Chen, H. Zeng, *Biomacromolecules* **2020**, *21*, 2409.

[4] A. Venkataraman, E. V. Amadi, Y. Chen, C. Papadopoulos, *Nanoscale Res Lett* **2019**, *14*, 220.

[5] B. W. Walker, R. Portillo Lara, E. Mogadam, C. Hsiang Yu, W. Kimball, N. Annabi, *Prog Polym Sci* **2019**, *92*, 135.

[6] Z. L. Pianowski, J. Karcher, K. Schneider, *Chemical Communications* **2016**, *52*, 3143.

[7] I. N. Lee, O. Dobre, D. Richards, C. Ballestrem, J. M. Curran, J. A. Hunt, S. M. Richardson, J. Swift, L. S. Wong, *ACS Appl Mater Interfaces* **2018**, *10*, 7765.

[8] K. P. Sonu, L. Zhou, S. Biswas, J. Klier, A. C. Balazs, T. Emrick, S. R. Peyton, *Langmuir* **2022**, *39*, 2659.

[9] Y. Feng, M. Taraban, Y. B. Yu, *Soft Matter* **2012**, *8*, 11723.

[10] T. Xiang, T. Lu, W. F. Zhao, C. S. Zhao, *Langmuir* **2019**, *35*, 1146.

[11] H. Gu, G. Wang, X. Cao, *J Appl Polym Sci* **2021**, *138*, 51509.

[12] M. S. A. Abdelaty, *J Polym Environ* **2021**, *29*, 3227.

[13] T. A. Asoh, S. Takai, H. Uyama, *Langmuir* **2022**, *38*, 5183.

[14] A. Bin Imran, T. Seki, Y. Takeoka, *Polym J* **2010**, *42*, 839.

[15] N. Park, J. Kim, *Advanced Intelligent Systems* **2020**, *2*, 1900135.

[16] R. Yoshida, *Bull Chem Soc Jpn* **2008**, *81*, 676.

[17] D. Wirthl, R. Pichler, M. Drack, G. Kettlguber, R. Moser, R. Gerstmayr, F. Hartmann, E. Bradt, R. Kaltseis, C. M. Siket, S. E. Schausberger, S. Hild, S. Bauer, M. Kaltenbrunner, *Sci Adv* **2017**, *3*, e1700053.

[18] J. Jian, Y. Xie, S. Gao, Y. Sun, C. Lai, J. Wang, C. Wang, F. Chu, D. Zhang, *Carbohydr Polym* **2022**, *294*, 119760.

[19] J. Ruokolainen, R. Mäkinen, M. Torkkeli, T. Mäkelä, R. Serimaa, G. ten Brinke, O. Ikkala, *Science (1979)* **1998**, *280*, 557.

[20] Z. Wang, Y. Cong, J. Fu, *J Mater Chem B* **2020**, *8*, 3437.

[21] A. K. Means, M. A. Grunlan, *ACS Macro Lett* **2019**, *8*, 705.

[22] X. Wang, Z. Wang, X. Wang, L. Shi, R. Ran, *Carbohydr Polym* **2021**, *257*, 117665.

[23] D. Zhang, J. Jian, Y. Xie, S. Gao, Z. Ling, C. Lai, J. Wang, C. Wang, F. Chu, M. J. Dumont, *Chemical Engineering Journal* **2022**, *427*, 130921.

[24] X. Zhao, X. Chen, H. Yuk, S. Lin, X. Liu, G. Parada, *Chem Rev* **2021**, *121*, 4309.

[25] W. Liu, H. Du, M. Zhang, K. Liu, H. Liu, H. Xie, X. Zhang, C. Si, *ACS Sustain Chem Eng* **2020**, *8*, 7536.

[26] A. Sharma, M. Thakur, M. Bhattacharya, T. Mandal, S. Goswami, *Biotechnology Reports* **2019**, *21*, e00316.

[27] C. Qian, T. A. Asoh, H. Uyama, *J Mater Chem B* **2020**, *8*, 2400.

[28] C. Qian, T. A. Asoh, H. Uyama, *Chemical Communications* **2018**, *54*, 11320.

[29] G. Sun, M. Zhang, J. He, P. Ni, *J Polym Sci A Polym Chem* **2009**, *47*, 4670.

[30] A. Darvishi, M. J. Zohuriaan Mehr, G. B. Marandi, K. Kabiri, H. Bouhendi, H. Bakhshi, *Des Monomers Polym* **2013**, *16*, 79.

[31] M. Gao, Y. Meng, C. Shen, Q. Pei, *Adv Mater* **2022**, *34*, 2109798.

[32] H. Kılıç, D. Ceylan Tuncaboylu, A. Argun, D. Öztürk Civelek, *ACS Appl Polym Mater* **2022**, *4*, 1717.

[33] Z. Chen, H. Wu, J. Fei, Q. Li, R. Ni, Y. Qiu, D. Yang, L. Yu, *RSC Adv* **2023**, *13*, 2649.

[34] A. Chakrabarty, Y. Teramoto, *ACS Appl Polym Mater* **2021**, *3*, 5441.

Chapter 3
Hydrogel Actuators with Gradient Distribution of Cellulose Nanocrystals for Controllable Bending Properties

3-1. Introduction

Stimuli-responsive hydrogel actuators with anisotropic structure have been increasingly used in the development of microtechnologies. These materials can undergo shape changes in response to stimuli, allowing for their use as manipulators,[1,2] sensors,[3,4] drug delivery devices,[5] and force generators.[6] Conventional anisotropic hydrogel actuators have a bilayer structure composed of responsive and non-responsive layers.[7] Bilayer-structured hydrogels are popular for their excellent response performance and simple production but often disintegrate owing to mismatch deformation at the layer interface after repeated flexion and extension.[8,9] Moreover, the requirement for adhesion between the layers complicates the production process. Therefore, anisotropic single-structured hydrogels are a desirable alternative.

Single-structured gradient hydrogels have been fabricated by the electrophoretic method,[10,11] ionoprinting,[12–14] and weak UV penetration.[15–17] The electrophoretic method is particularly useful for creating gradient structures because of the increased controllability, ease of processing, and unnecessity of using specialized devices.[18] Two primary criteria must be met for electrophoresis to be utilized: (1) a charged component must be introduced, and (2) the gelation time should be longer than the migration time of the charged component.[19] In this method, the application of an electric field induces the migration of charged particles toward one side of the hydrogel, creating a gradient distribution of particles, and a gelation reaction is performed to fix the gradient structure. The resulting anisotropic structures impart an actuating function to stimuli-responsive hydrogels.

Cellulose nanocrystals (CNCs) are promising materials for creating the gradient structure in hydrogels by electrophoresis because their surfaces have negatively charged sulfate half-esters. Application of electric field have been a useful way to control the alignment of CNCs to realize functions in materials. [20–22] This method is often used for single CNCs systems and coatings.[23–25] By combining CNC with different materials, it is possible to expand the range of functions utilizing electrophoresis.[26–28] CNCs are widely used as reinforcement fillers in polymeric composite materials, enhancing the mechanical strength of the composite by improving its energy

adsorption characteristics. Thus, it is postulated that a gradient distribution of CNCs could locally influence the deswelling behavior of stimuli-responsive hydrogels, resulting in stimulus-induced curvature. Moreover, since the crystallinity of cellulose depends on its origin, various sizes and dimensions of CNCs can be obtained from different natural cellulosic sources.[29–31] Therefore, control of the dimensions of the CNCs and the electrophoresis conditions will contribute to controllable bending behaviors in hydrogels.

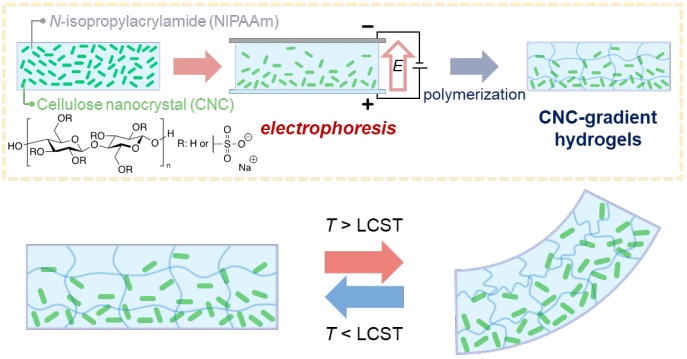

Figure 3-1. Conceptual illustration of gradient nanocomposite hydrogel.

In this study, a gradient hydrogel actuator was developed through the electrophoresis method, using CNCs as the migratable component. Recently, Chang *et al.* have reported high-performance gradient hydrogel actuators that utilizes high-strength CNC derived from marine animals.[26,27] While, from the perspective of utilization of readily available renewable resources, it is preferable to use plant-derived CNCs. Hence, the author prepared CNCs from different sources from plant-derived raw materials to reveal the dimensional effect of CNC on the performances. Poly(*N*-isopropylacrylamide) (PNIPAAm), a widely studied thermoresponsive hydrogel, was selected as the stimuli-responsive base material.[32–38] This hydrogel swells below a lower critical solution temperature (LCST) and shrinks above this temperature. Electrophoresis was performed under varying conditions to generate gradient structures, and subsequent photopolymerization of *N*-isopropylacrylamide (NIPAAm) and cross-linker was carried out to obtain an anisotropic thermoresponsive hydrogel with spatially fixed CNCs. Owing to the anisotropic distribution of the CNCs and the sharp volume phase transition of the PNIPAAm hydrogel, the CNC-gradient hydrogels exhibited significant bending capabilities (**Figure 3-1**). Different bending angles and velocities were evaluated to determine optimal preparation conditions.

3-2. Experimental Section

Materials

Nata de Coco seasoned with syrup was purchased from Tengu Kanzume Co. Ltd. (Japan). An Advantec No. 5C filter paper was purchased from Toyo Roshi Co. Ltd. (Japan) and cut into small

pieces for use. *N*-isopropylacrylamide (NIPAAm), sodium hydroxide (NaOH), and 64% sulfuric acid (H_2SO_4) were purchased from Wako Pure Chemical Industries Ltd. (Japan). 2-hydroxy-4'-(2-hydroxyethoxy)-2-methylpropiophenone (Irgacure® 2959) was obtained from Tokyo Chemical Industry Co. Ltd. Poly(ethylene glycol) dimethacrylate (PEGDMA) with an approximate number-average molecular weight of 750 was supplied by Aldrich (USA). Prior to use, the NIPAAm monomer was purified by dissolution in methanol at 25 °C and recrystallization at 4 °C, before being collected by vacuum filtration.

Preparation of filter paper—based cellulose nanocrystal and bacterial cellulose nanocrystal suspensions

FCNC and BCNC suspensions were produced from the filter paper and Nata de Coco, respectively. CNC suspensions are typically prepared in two steps, namely purification and acidic hydrolysis. The FCNC suspensions were not purified and only underwent acidic hydrolysis. Purification of the Nata de Coco was partially based on a previous report.[39] The Nata de Coco was first rinsed repeatedly with deionized (DI) water to remove seasonings and other impurities. The rinsed Nata de Coco was then heated in a 2 wt% NaOH solution at 80 °C for 1 h, then washed repeatedly in DI water to yield refined and neutralized Nata de Coco. The refined Nata de Coco was then blended in a laboratory blender for around 15 min at 25 °C to produce a bacterial cellulose paste. Finally, the paste was lyophilized for 48 h to remove moisture prior to the acidic hydrolysis step.

The dried bacterial cellulose and filter paper were used as the source materials for cellulose. An acidic hydrolysis protocol referred to in a previous report[40] and a modification thereof[41] were used to obtain the appropriate CNC suspensions. In brief, the cellulose was hydrolyzed with sulfuric acid at a ratio of 1:14 g mL^{-1} in a 64% H_2SO_4 solution for 45 min at 45 °C under vigorous mechanical stirring. The reaction was terminated by the addition of 10-fold DI water and cooling in an ice bath. The excess acidic solution was removed by centrifugation at 9000 rpm at 4 °C for 10 min and decanting the supernatant. This step was repeated until optical turbidity was observed in the supernatant, at which point the turbid supernatant was collected. The gathered supernatant was dialyzed (MWCO 10,000) against DI water to obtain a neutral CNC suspension.

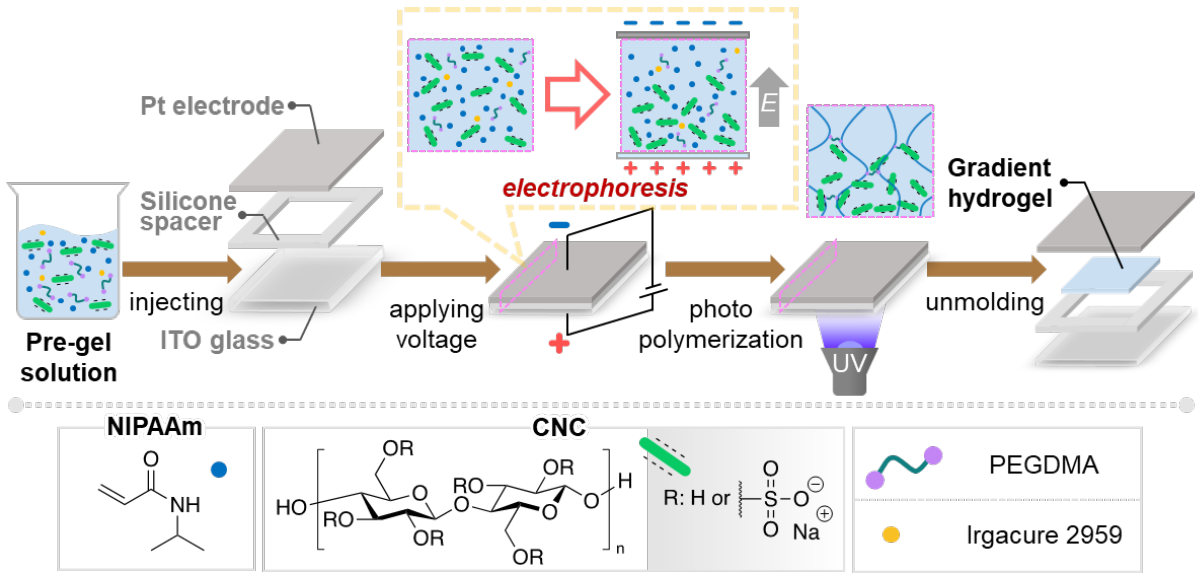

Figure 3-2. Schematic illustration of preparation of gradient nanocomposite hydrogel.

Fabrication of gradient nanocomposite hydrogels

PNIPAAm-CNC gradient nanocomposite hydrogels were prepared by applying an electric field to a CNC suspension containing NIPAAm, cross-linker, and initiator, as shown in **Figure 3-2**. A 10 g mixture was prepared by mixing 3 wt% CNC suspension in DI water with NIPAAm (0.71 g, 7 mmol), PEGDMA (0.1 g, 0.14 mmol), and Irgacure® 2959 (15 mg, 0.07 mmol). After degassing for 10 min in a vacuum pump, the suspension was transferred to a mold (20 × 20 × 2 mm) where it was subjected to an electric voltage (6 V) for 10-40 s. The mold was composed of indium tin oxide (ITO) glass as the cathode, a platinum plate as the anode, and silicone rubber as the spacer. After removing the voltage and polymerizing the suspension in chilled water for 1 h under UV irradiation (30 mW cm^{-2}), a PNIPAAm-CNC gradient nanocomposite hydrogel was acquired. The resulting hydrogel was immersed in DI water for several days to remove unreacted chemicals and byproducts and to maintain a hydrated state. The resultant composite hydrogels presented in this study are designated by "C*p*V*q*T*r*," where C, V, and T represent the CNC type, applied voltage, and electrophoresis time, respectively, and *p*, *q*, and *r* are replaced by the concentration of CNCs (wt%), the applied voltage (V), and the electrophoresis time (s), respectively (for specific hydrogels, C is replaced by the abbreviation for the CNC source, namely F for filter paper and B for Nata de Coco).

Characterization

The morphologies and dimensions of the hydrolyzed CNCs were analyzed by atomic force microscopy (AFM, SPI3800N/SPA-400, Seiko Instruments Inc., Tokyo, Japan). A highly diluted CNC suspension (approximately 1.0×10^{-5} wt%) was deposited on the mica surface. After adsorption onto the surface, the sample was air-dried. The CNCs were analyzed in contact mode. The morphology of the cross-section of lyophilized hydrogels was observed by SEM (Hitachi SU3500N, Japan) with an accelerating voltage of 15 kV. Wide-angle X-ray scattering (WAXS) was performed utilizing BL40B2 beamline (Spring-8, Japan). The wavelength was at 0.1 nm and flat-panel detector was used for the collection of data. Mending tape was used to hold the sample onto the beamline. The charged surface and hydrodynamic size of the CNCs were measured with a ζ-potential and particle size analyzer (ELSZ-2000 Series, Otsuka Electronics Co. Ltd., Japan) to determine the successful preparation of the CNC suspensions. The suspensions containing 1 wt% CNCs and measurements were performed at 25 °C. The functional group profile of the lyophilized composite hydrogels was analyzed via attenuated total reflection Fourier transform infrared (ATR-FTIR) spectroscopy (Nicolet iS 5, Thermo Scientific, USA) coupled with an iD5 ATR attachment. The mechanical properties of hydrogels were examined using an oscillation frequency sweep by using a rheometer (Hakke RheoStress 6000, Thermo Scientific, USA) with a 20 mm parallel-plate configuration. Experiments were conducted at 25 °C with a constant strain (γ) of 0.01 over a range of frequency (ω) of 0.1-10 rad s^{-1}.

Measurement of deswelling behavior

The deswelling behavior of the hydrogels was evaluated by the following method. The prepared hydrogels were punched into disc shapes with approximate radius and thickness of 5 and 2 mm, respectively, and were then placed in a water bath at 25 °C until they reached equilibrium. The hydrogels were then swiftly moved into a 50 °C water bath. The diameters of the hydrogels were measured immediately from the onset of heating for a specified duration of time. Each presented result is an average derived from three independent measurements. The deswelling ratios were calculated as the ratio of the diameter of the hydrogel under a given time (D_t) at 50 °C to the equilibrated hydrogels at 25 °C (D_0) as D_t/D_0. To analyze the deswelling behavior empirically, a first-order rate analysis related to the time dependency of deswelling was employed,[42–45] as shown in **eq 1**, for which D_t is the diameter of the equilibrated hydrogel at a response time t (min) in 50

°C, D_{eq} is the equilibrium diameter of the swollen hydrogel at 50 °C, and k is a rate constant. This formulation was used to determine the deswelling rate constant. The kinetics of deswelling process was described in terms of the slope of a plot of $\ln\left(\frac{D_t - D_{eq}}{D_0 - D_{eq}}\right)$ against t.

$$\left|\frac{D_t - D_{eq}}{D_0 - D_{eq}}\right| \sim \frac{8}{\pi^2} e^{-kt} \quad (1)$$

Bending angle measurement

The hydrogels were divided into 20 × 10 × 2 mm segments. The width side of the hydrogel was fixed while the other side hung freely in the water. The hydrogels were soaked in a 25 °C water bath to achieve equilibrium. They were subsequently placed in DI water at 50 °C and the response time and bending angle were monitored. The protocol used to measure the bending angle was the same as that in a previous report.[46] Bending behavior was evaluated by plotting the bending angle against the response time.

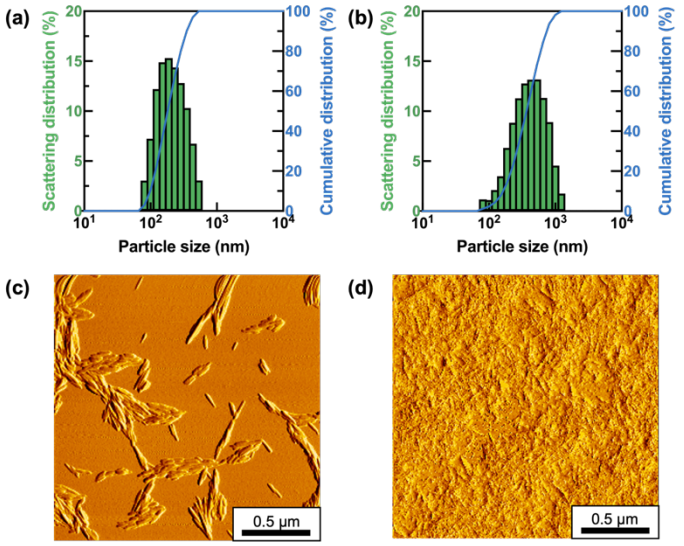

Figure 3-3. Dimension and morphology of CNC samples. Statistical results of particle size distribution of (a) FCNC and (b) BCNC and AFM images of (c) FCNC and (d) BCNC.

3-3. Results and Discussion

Morphologies and Surface Charges of CNCs

Negatively charged CNCs were prepared to induce the formation of a gradient structure in the material by electrophoresis. The average particle sizes of the filter paper–based (FCNC) and bacterial (BCNC) cellulose nanocrystal measured by particle size analyzer were 178.9 ± 0.2 and 336.6 ± 0.2 nm, respectively (**Figure 3-3a and b**). Smaller CNCs were therefore obtained from the filter paper than from the Nata de Coco. The morphology and

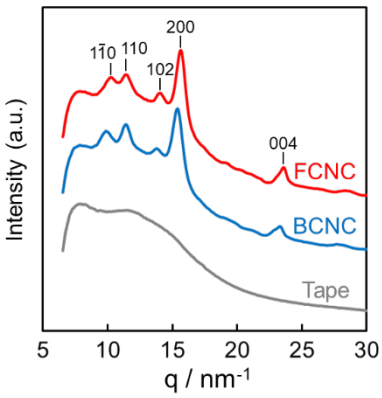

Figure 3-4. WAXS spectra of FCNC (red), BCNC (blue), and mending tape (sample holder, gray).

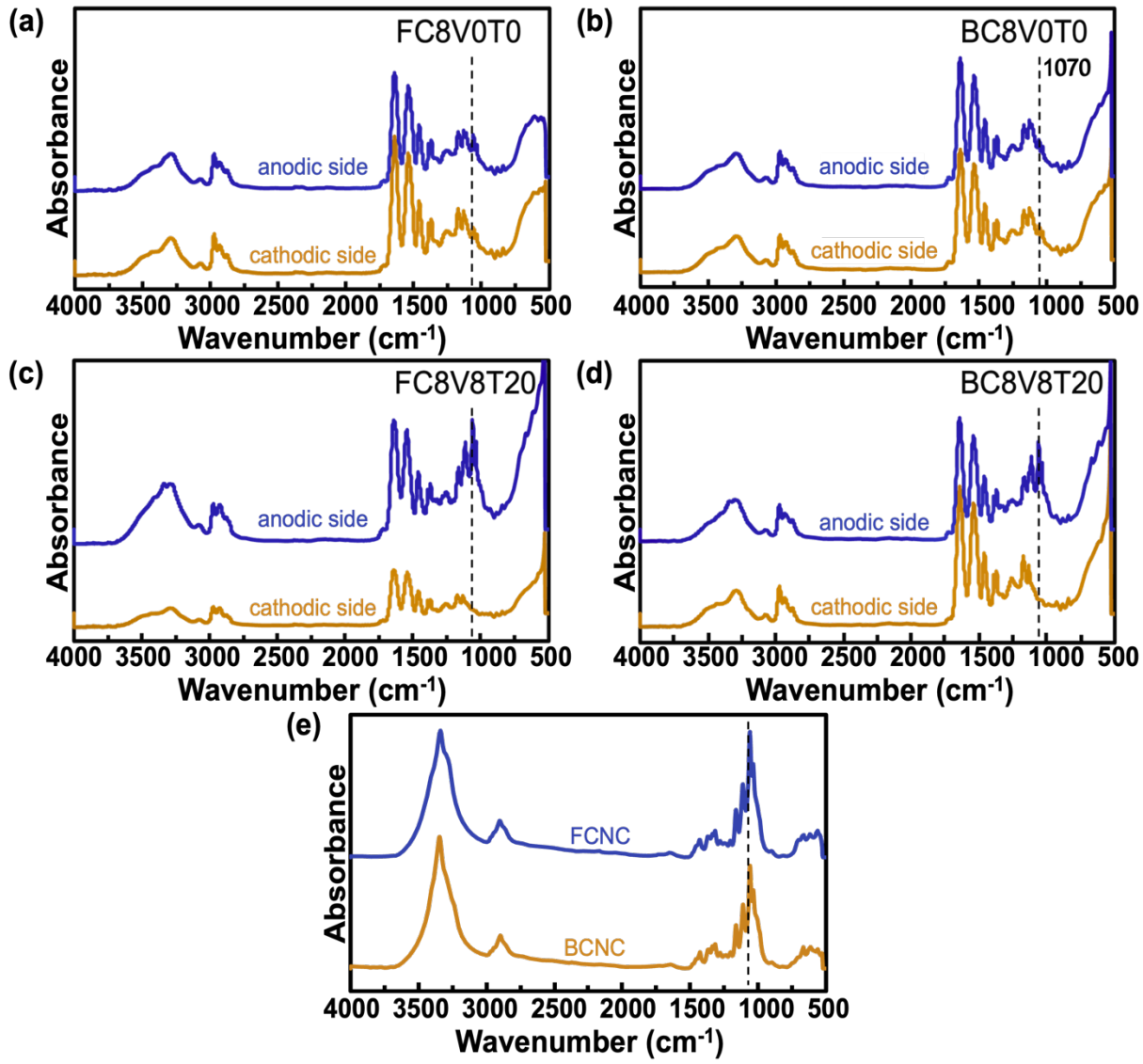

Figure 3-5. IR spectra of composite hydrogel based on FCNC (a,b) without and (c,d) with electrophoresis (FC8V0T0 and FC8V8T20), and (e) dried FCNC (violet) and BCNC (brown).

dimensions of the CNCs were observed by AFM. The FCNCs and BCNCs both exhibited uniform needle-like structures with lengths of 105.0 ± 0.6 and 382.6 ± 0.2 nm, respectively, consistent with the dynamic light scattering (DLS) measurements (**Figure 3-3c and d**). The results of wide-angle X-ray scattering (WAXS) revealed that FCNC and BCNC has similar crystalline structures that are characteristic in CNC (**Figure 3-4**). Through hydrolysis with sulfuric acid, the CNC surface is modified with negatively charged sulfate half-esters which can be analyzed by ζ-potential analysis. Both the FCNCs and BCNCs exhibited negative ζ-potentials of -33.48 and -34.44 mV,

respectively. Thus, the negative charge of the CNC surface can be used to manipulate the distribution of CNCs along the thickness of the composite hydrogel by electrophoresis.

Preparation of CNC-gradient composite hydrogels

Hydrogel networks were prepared by radical photopolymerization of the NIPAAm and cross-linker solutions containing CNCs. Gradient distributions of the CNC particles were controlled through electrophoresis, using a transparent ITO electrode and a platinum plate as the working anode and cathode, respectively. After injecting the pre-gel solution into the electrode mold, a direct current electric field was applied, forcing the negatively charged CNCs to migrate toward the anodic side and generating a gradient structure. In addition, the dispersibility of CNC in the pre-gel solution was sufficiently high, minimizing significant sedimentation of CNC on the bottom during polymerization. The solution was then subjected to UV irradiation from the bottom surface through the ITO glass electrode, to obtain CNC-gradient composite hydrogels (**Figure 3-2**).

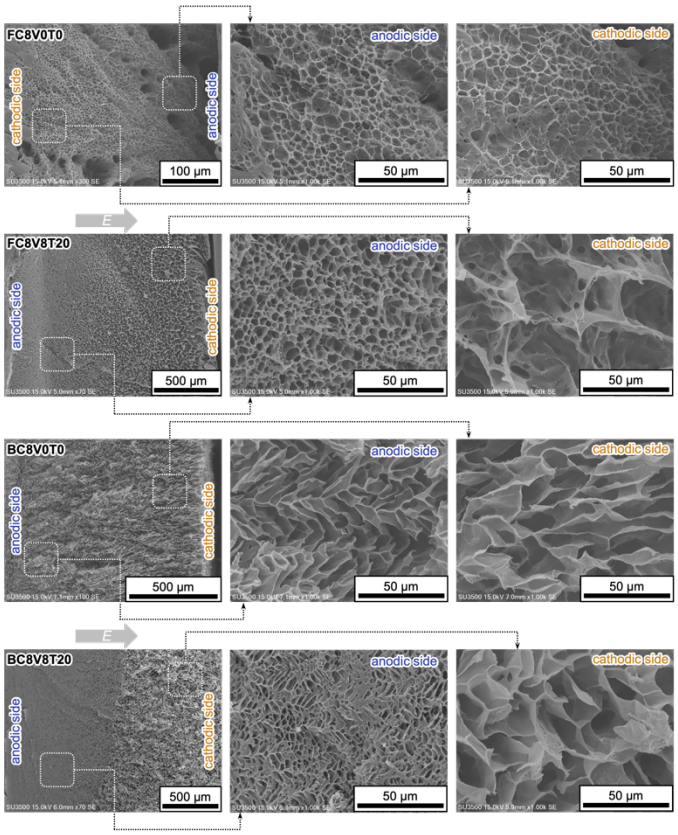

Figure 3-6. SEM images of the morphology of FC8V0T0, FC8V8T20, BC8V0T0, and BC8V8T20 hydrogels, with enlarged images at anodic and cathodic sides of each hydrogel.

The cathodic and anodic sides of the acquired hydrogels were characterized by FTIR spectroscopy (**Figure 3-5**). C0V0T0 samples exhibited identical spectra at both sides of the hydrogel. Sample FC8V0T0, which was prepared without electrophoresis, similarly exhibited identical spectra at both sides (**Figure 3-5**). These results indicate uniform dispersion of the CNCs in these hydrogels. In contrast, FC8V8T20, prepared under the application of an electric field, exhibited a peak at approximately 1070 cm^{-1}, only on its anodic side. A similar trend was observed

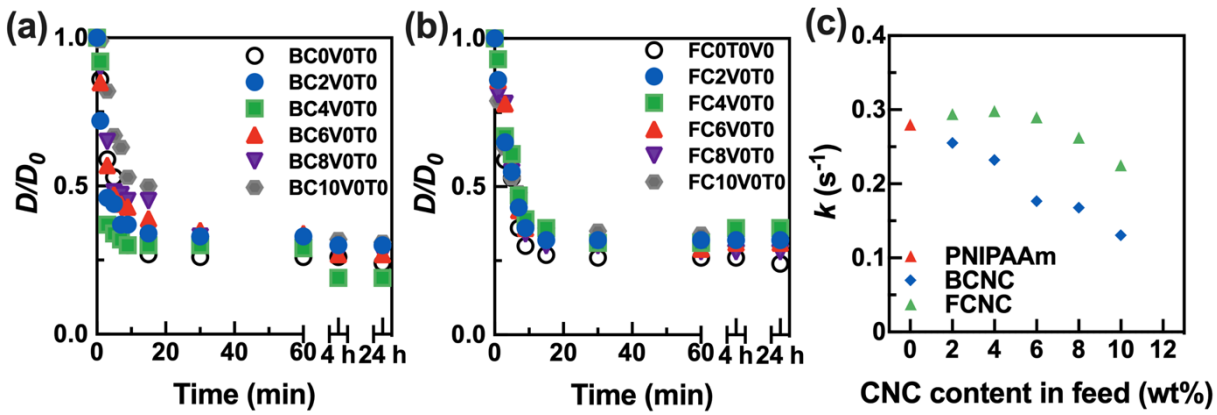

Figure 3-7. Time-dependent swelling ratio of uniform composite hydrogel prepared with different feed (a) BCNC and (b) FCNC contents, and (c) deswelling rate constant, *k*, of those hydrogels with and without BCNC or FCNC when temperature stepped from 25 to 50 °C.

in the hydrogels with BCNCs (**Figure 3-5a and b**). When comparing the spectra with those of CNC powder, it is apparent that the peak at 1070 cm^{-1} is attributed to C–H bending vibration of CNC (**Figure 3-5e**).[47,48] These results indicate that there was a higher concentration of CNCs at the anodic side than at the cathodic side, confirming that electrophoresis is an effective method of forming CNC gradients in composite hydrogels.

To further confirm the gradient structure, the morphology of the composite hydrogels was investigated using scanning electron microscopy (SEM) (**Figure 3-6)**. In FC8V0T0 hydrogel, prepared without electrophoresis, the relatively similar network structures were observed both on the anodic and cathodic sides. On the other hand, FC8V8T20 hydrogel, prepared under electrophoresis, exhibited significant difference in the network structure on the anodic and cathodic sides. The anodic side with greater existence of CNC exhibited a dense network structure with small pores, while a loose network was observed on the cathodic side with less CNC. These results suggest that the controlling the distribution of CNC by electrophoresis enables to create the gradient structure of the hydrogels.

Deswelling properties

The deswelling process in non-gradient composite hydrogels was examined by swiftly elevating the temperature of the aqueous environment from 25 to 50 °C, beyond the transition temperature of PNIPAAm. After being submerged in water at 50 °C, the composite hydrogels shrunk and became opaque. The swelling ratios, defined by D/D_0, demonstrated the time-

dependence of deswelling behavior in the composite hydrogels. The D/D_0 of the FCNC-based composite hydrogels decreased dramatically over time (**Figure 3-7b**). These hydrogels demonstrated a fast initial deswelling response, which plateaued around the 15-min point of the first period. After this point, the D/D_0 of the FCNC-based composite hydrogels remained stable for 24 h. The BCNC-based composite hydrogels also exhibited fast initial deswelling behavior (**Figure 3-7a**).

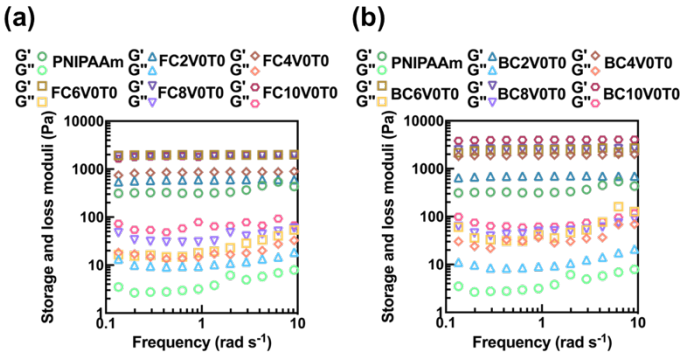

Figure 3-8. Rheological properties of (a) FCNC and (b) BCNC gradient hydrogels.

Furthermore, the deswelling rate constants, k, were calculated to analyze the deswelling kinetics (**Figure 3-7c**). It was discovered that the k of both types of hydrogels decreased with increasing CNC content. This was attributed to the large amounts of CNCs in the composite hydrogels having a reinforcing effect, restricting the hydrogel from changing its shape.[49] A similar effect was observed from the comparison of the k values of the FCNC– and BCNC-based hydrogels; larger BCNCs provided a reinforcing effect preventing the deswelling of the composite hydrogel, resulting in smaller k values for these hydrogels compared with those of the FCNC-based hydrogels. The k value for the FCNC-based composite hydrogels decreased dramatically when the amount of FCNCs increased above 6 wt%. Meanwhile the k value for the BCNC-based hydrogels decreased even at a BCNC loading of 2 wt% and decreased significantly with loadings above 6 wt%. Increasing the number of CNCs resulted in slower deswelling, indicating that the CNCs acted as a reinforcing filler and suppressed the dehydration of the hydrogels. The rheological properties of the non-gradient composite hydrogels also showed that the stiffness of the hydrogels increased with increasing concentration of CNCs, which supports the reinforcing effect of CNCs as fillers (**Figure 3-8**). These results show that the deswelling process was affected both by the dimensions of the CNCs from the different sources and the CNC concentration in the composites. These results strongly suggest that a gradient distribution of CNCs leads to differences in deswelling speed and may thus affect the bending behavior of the hydrogels in which they are incorporated.

Bending properties of CNC-gradient composite hydrogels

Preparation parameters were varied to investigate the thermoresponsive bending characteristics of CNC-gradient composite hydrogels. The hydrogels were transferred to water at temperatures ranging from 25 to 50 °C, and bending properties were analyzed by the resulting hydrogel bending angle of ∠ POQ, defined in **Figure 3-9**.

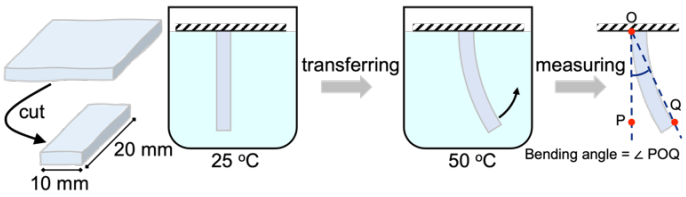

Figure 3-9. Schematic illustration of bending angle measurement.

Increasing the temperature from 25 to 50 °C caused the hydrogels to gradually bend into a semicircular shape over approximately 4 min of heating (**Figure 3-10**). The bending angle increased over time, reaching approximately 80° after 6 min for sample FC8V6T20. The effects of varying the preparation conditions on the bending properties were then evaluated, starting with the electrophoresis duration, as shown in **Figure 3-11**. The FCNC concentration and voltage were fixed at 8 wt% and 6 V, respectively, except for case FC8V0T0, which did not undergo electrophoresis. FC8V0T0 bent to 20° and did not bend significantly further even under continuous heating. Conversely, FC8V6T10, subjected to 10 s of electrophoresis, exhibited gradual bending under heating, bending to around 30° within 5 min. Moreover, in the case of FC8V6T20, subjected to 20 s of electrophoresis, the bending angle reached 80°. These results indicate that an enhanced gradient distribution of CNCs may lead to faster bending at larger angles. They also suggest that the gradient structure itself contributes strongly to the bending because the side with lower CNC concentration shrunk faster than that with high CNC concentration, resulting in the curving of the hydrogel. While the hydrogel with

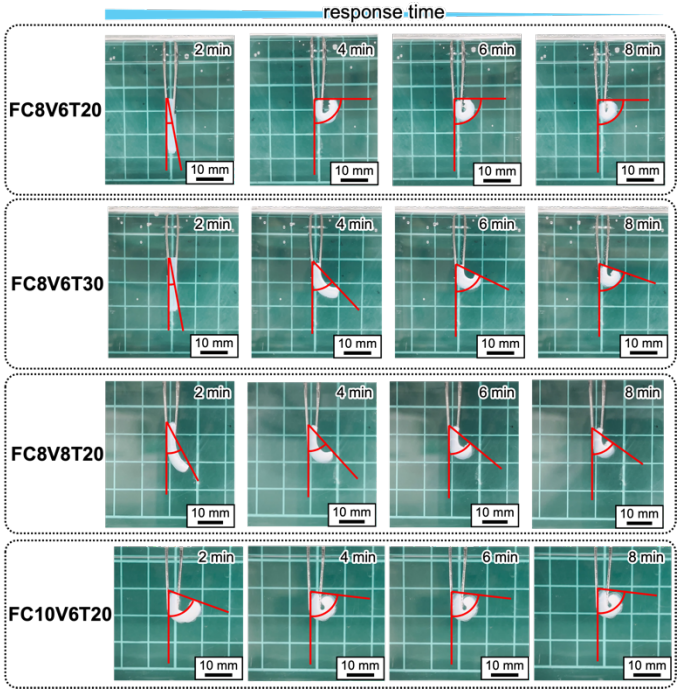

Figure 3-10. Sequence of gradient hydrogel snapshots with different electrophoresis time, applied voltage and amount of feed FCNC in fabrication of gradient hydrogel.

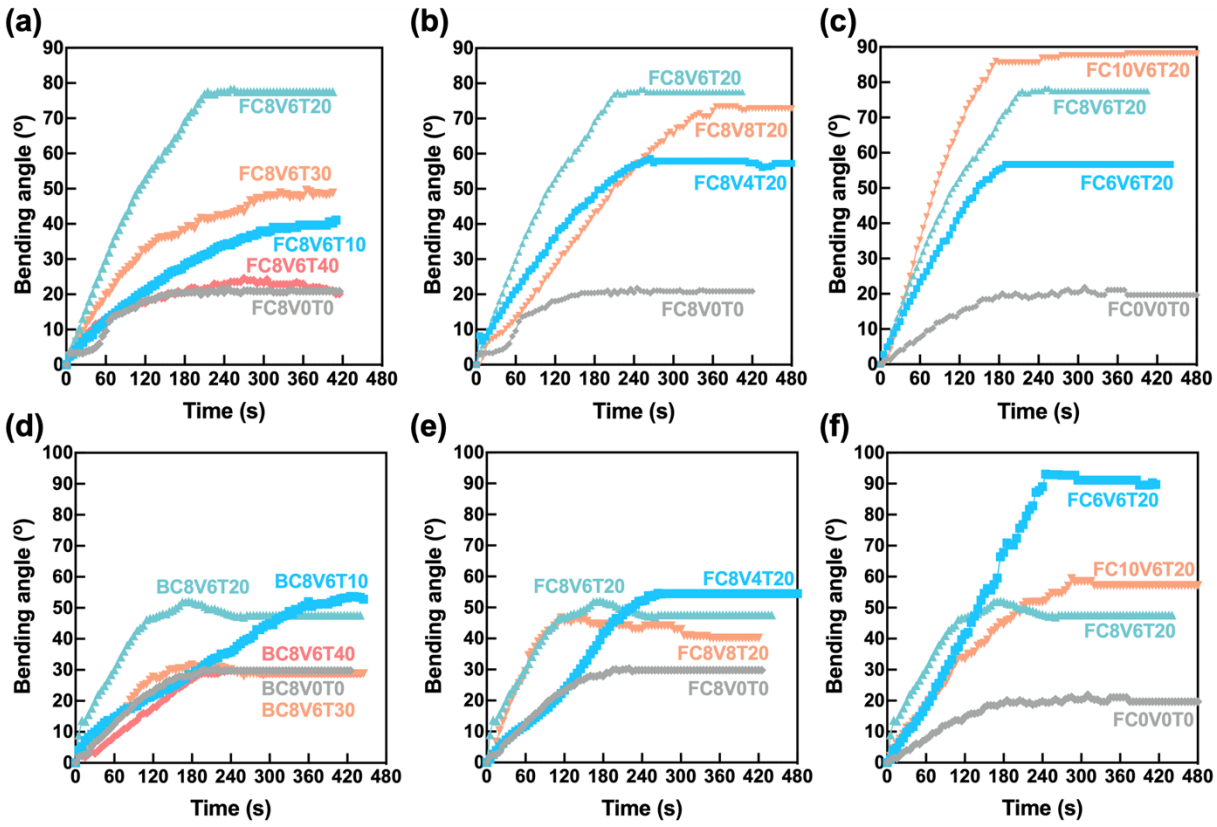

Figure 3-11. Plot of bending angle against response time of gradient hydrogels, prepared from FCNC and BCNC with various conditions of (a,d) electrophoresis time, (b,e) applied voltage, and (c,f) amount of FCNC in feed, respectively.

uniformly distributed CNCs also bent to some extent, possibly due to the unidirectional UV irradiation during polymerization, it did not exhibit significant bending compared to that of the gradient hydrogels. Further increasing the electrophoresis time to 30 and 40 s caused the bending angle of the hydrogel to decrease (**Figure 3-10**). The bending behavior of FC8V6T40 was similar to that of FC8V0T0. This suggests that longer electrophoresis times may suppress bending by causing a localization of FCNCs on the anodic side, stiffening this portion of the hydrogel. The BCNC-gradient composite hydrogels also showed similar tendencies in bending properties (**Figure 3-11d**). Compared to the FCNC-gradient composite hydrogels, BC8V6T20 exhibited a smaller maximum bending angle (approximately 50°). This was attributed to the longer lengths of BCNCs causing a more prominent increase in the stiffness of the hydrogel at the anodic side, suppressing bending, while the FCNCs with shorter lengths had a relatively smaller reinforcing effect and provided appropriate gradient structures which did not hinder bending. From these

results, an electrophoresis time of 20 s was suggested to be further investigated for each type of gradient composite hydrogel to realize fast and significant bending.

The effects of varying the voltage of the applied electric field on the bending behaviors of the CNC-gradient hydrogels were then investigated. With increasing applied voltage, the FCNC-gradient composite hydrogels exhibited larger maximum bending angles and higher bending speeds (**Figure 3-11b**). FC8V4T20 gradually bent to approximately 60° under continuous heating. Increasing the applied voltage to 6 V (FC8V6T20) produced a bending angle of 80° within 3 min (**Figure 3-10**). These results indicate that increasing the applied voltage promotes more optimal CNC distribution gradients for bending behaviors. Since the migration rate of the CNCs is proportional to the magnitude of the electric field, higher voltages enhance the anisotropy of the distribution of CNCs in composite hydrogels. When the applied voltage was further increased to 8 V, the bending rate decreased owing to the increased rigidity of the CNC-dense layer of the hydrogel. The BCNC-gradient hydrogels showed a similar trend of increased maximum bending angles with increasing applied voltage, particularly for BC8V6T20 (**Figure 3-11e**). Compared at similar CNC concentrations, the FCNC-gradient hydrogels exhibited more rapid responses and higher bending angles than those of the BCNC-gradient hydrogels. These results are in good agreement with those of varying the electrophoresis time of the hydrogels. In both cases, the increased stiffness of the BCNC-gradient hydrogels inhibited fast bending and limited the maximum bending angle. A voltage of 6 V was selected for further study, based on the optimal bending speeds and angles achieved with this voltage.

Lastly, the effect of initial CNC concentration on the bending properties was investigated. Without CNCs (as a neat PNIPAAm hydrogel), C0T0V0 exhibited a low bending rate and a small maximum bending angle of approximately 20°. When either BCNCs or FCNCs were introduced, the bending speed increased, and the maximum bending angle was significantly enhanced (50–90°) (**Figure 3-11c and f**). This confirmed that incorporating and controlling the distribution of CNCs by electrophoresis is essential for fabricating gradient composite hydrogels. The bending ability of FCNC-gradient hydrogels increased with increasing FCNC concentration, and the largest bending angle and highest bending speed were realized at 10 wt% FCNCs (FC10V6T20). In the case of BCNCs, the hydrogel with 6 wt% BCNCs exhibited the highest bending speed and largest bending angle. Increasing the amount of BCNCs led to a decrease in the bending angle from approximately 90 to 50°. This was consistent with the previous result, in that an excessively local

increase of CNC concentration on one side of the hydrogel decreased the bending capability. The bending properties of CNC-gradient gels are therefore affected by both the overall gradient structure and the flexibility of the CNC-rich layer. Processing conditions should therefore be optimized depending on the size and dimensions of the CNCs to be used.

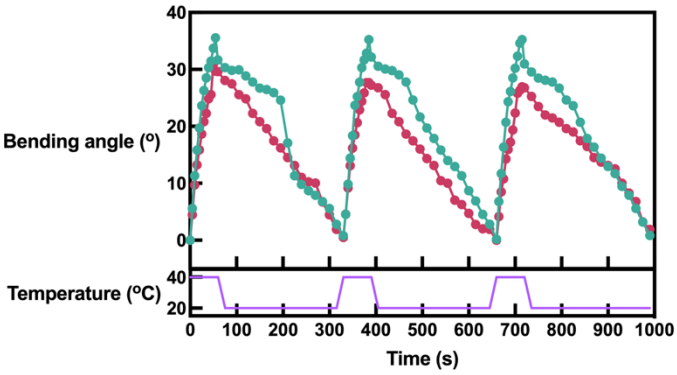

Figure 3-12. Cycles of bending and straightening in FC10V6T20 (green) and BC6T8V20 (magenta) gels with temperature program (lilac).

Furthermore, the repetitive process of heating and cooling in optimized gradient hydrogel was performed to evaluate the reproducibility of the actuating response (**Figure 3-12**). Both gradient hydrogels with FCNC and BCNC displayed reversible bending and straightening cycles by heating and cooling, respectively.

In summary, by adjusting the fabrication conditions of CNC-gradient hydrogels, the bending properties thereof can be optimized through control of the distribution of CNCs within the hydrogel. The electrophoresis method, by which CNCs are distributed within the hydrogels via an applied electric field, can be used to develop gradient hydrogels with significant bending abilities. Large bending angles and rapid bending response can be realized by optimizing the electrophoresis time, voltage, and CNC concentration. Shorter-length CNCs are also beneficial for optimal flexibility of the CNC-rich layer, as they provide less of a reinforcement effect. Moreover, the bending−straightening behavior of the hydrogels was able to be controlled by heating and cooling, exhibiting reversibility.

3-4. Conclusions

Hydrogel actuators were successfully fabricated from gradient composite hydrogels prepared by electrophoresis. The hydrogels contained a gradient distribution of FCNCs or BCNCs in a PNIPAAm network. The gradient structure was optimized to produce hydrogel actuators with high bending speeds and large bending angles by adjusting the electrophoresis time and voltage, and the CNC concentration. The bending behaviors of the hydrogels were attributed to the gradient distribution of the CNCs which causes different degrees of deswelling of the hydrogel upon heating. Bending behaviors were also affected by the size distribution of the CNCs, whereby

smaller CNCs helped to maintain the flexibility of CNC-rich layers, improving the bending abilities. Moreover, the reversible bending−straightening cycles were achieved by heating and cooling. The author's novel process, therefore, shows how to facilely produce responsive single-layer gradient hydrogel actuators with controllable bending properties.

3-5. References

[1] C. Yao, Z. Liu, C. Yang, W. Wang, X. J. Ju, R. Xie, L. Y. Chu, *Adv Funct Mater* **2015**, *25*, 2980.

[2] Z. Sun, C. Song, J. Zhou, C. Hao, W. Liu, H. Liu, J. Wang, M. Huang, S. He, M. Yang, *Macromol Rapid Commun* **2021**, *42*, 2100499.

[3] Q. Guo, Y. Liu, J. Liu, Y. Wang, Q. Cui, P. Song, X. Zhang, C. Zhang, *Chemistry of Materials* **2022**, *34*, 5165.

[4] F. Diehl, S. Hageneder, S. Fossati, S. K. Auer, J. Dostalek, U. Jonas, *Chem Soc Rev* **2022**, *51*, 3926.

[5] Z. Han, P. Wang, G. Mao, T. Yin, D. Zhong, B. Yiming, X. Hu, Z. Jia, G. Nian, S. Qu, W. Yang, *ACS Appl Mater Interfaces* **2020**, *12*, 12010.

[6] K. Sano, Y. Ishida, T. Aida, *Angewandte Chemie* **2018**, *130*, 2558.

[7] D. H. Gracias, *Curr Opin Chem Eng* **2013**, *2*, 112.

[8] J. Li, Z. Xu, Y. Xiao, G. Gao, J. Chen, J. Yin, J. Fu, *J Mater Chem B* **2018**, *6*, 257.

[9] S. Yang, K. Khare, P. C. Lin, *Adv Funct Mater* **2010**, *20*, 2550.

[10] Y. Tan, D. Wang, H. Xu, Y. Yang, X. L. Wang, F. Tian, P. Xu, W. An, X. Zhao, S. Xu, *ACS Appl Mater Interfaces* **2018**, *10*, 40125.

[11] Y. Yang, Y. Tan, X. Wang, W. An, S. Xu, W. Liao, Y. Wang, *ACS Appl Mater Interfaces* **2018**, *10*, 7688.

[12] A. B. Baker, D. F. Wass, R. S. Trask, *Sens Actuators B Chem* **2018**, *254*, 519.

[13] E. Palleau, D. Morales, M. D. Dickey, O. D. Velev, *Nat Commun* **2013**, *4*, 2257.

[14] B. Y. Wu, X. X. Le, Y. K. Jian, W. Lu, Z. Y. Yang, Z. K. Zheng, P. Théato, J. W. Zhang, A. Zhang, T. Chen, *Macromol Rapid Commun* **2019**, *40*, e1800648.

[15] X. X. Le, Y. C. Zhang, W. Lu, L. Wang, J. Zheng, I. Ali, J. W. Zhang, Y. J. Huang, M. J. Serpe, X. T. Yang, X. D. Fan, T. Chen, *Macromol Rapid Commun* **2018**, *39*, 1800019.

[16] L. Hua, M. Xie, Y. Jian, B. Wu, C. Chen, C. Zhao, *ACS Appl Mater Interfaces* **2019**, *11*, 43641.

[17] Z. Shao, S. Wu, Q. Zhang, H. Xie, T. Xiang, S. Zhou, *Polym Chem* **2021**, *12*, 670.

[18] N. Zinkovska, J. Smilek, M. Pekar, *Polymers (Basel)* **2020**, *12*, 966.

[19] X. Xia, Y. Yang, X. Zhou, E. Liu, S. Xu, *Carbohydr Polym* **2022**, *289*, 119473.

[20] D. Bordel, J. L. Putaux, L. Heux, *Langmuir* **2006**, *22*, 4899.

[21] Y. Habibi, T. Heim, R. Douillard, *J Polym Sci B Polym Phys* **2008**, *46*, 1430.

[22] A. Kadimi, K. Benhamou, Z. Ounaies, A. Magnin, A. Dufresne, H. Kaddami, M. Raihane, *ACS Appl Mater Interfaces* **2014**, *6*, 9418.

[23] S. Atifi, M. N. Mirvakili, C. A. Williams, M. M. Bay, S. Vignolini, W. Y. Hamad, *Advanced Materials* **2022**, *34*, 2109170.

[24] T. Kasuga, T. Saito, H. Koga, M. Nogi, *ACS Nano* **2022**, *16*, 18390.

[25] Q. Chen, U. P. de Larraya, N. Garmendia, M. Lasheras-Zubiate, L. Cordero-Arias, S. Virtanen, A. R. Boccaccini, *Colloids Surf B Biointerfaces* **2014**, *118*, 41.

[26] K. Mo, M. He, X. Cao, C. Chang, *J Mater Chem C Mater* **2020**, *8*, 2756.

[27] K. Mo, J. Lin, P. Wei, J. Mei, C. Chang, *J Mater Chem C Mater* **2021**, *9*, 10295.

[28] L. Reid, W. Y. Hamad, *ACS Appl Polym Mater* **2022**, *4*, 598.

[29] S. Beck-Candanedo, M. Roman, D. G. Gray, *Biomacromolecules* **2005**, *6*, 1048.

[30] X. M. Fan, H. Y. Yu, D. C. Wang, J. Yao, H. Lin, C. X. Tang, K. C. Tam, *ACS Appl Mater Interfaces* **2019**, *11*, 48192.

[31] I. Leppänen, A. Hokkanen, M. Österberg, M. Vähä-Nissi, A. Harlin, H. Orelma, *Cellulose* **2022**, *29*, 8551.

[32] G. Stoychev, S. Zakharchenko, S. Turcaud, J. W. C. Dunlop, L. Ionov, *ACS Nano* **2012**, *6*, 3925.

[33] H. Lin, S. Ma, B. Yu, X. Pei, M. Cai, Z. Zheng, F. Zhou, W. Liu, *Chemistry of Materials* **2019**, *31*, 9504.

[34] J. Liu, W. Xu, Z. Kuang, P. Dong, Y. Yao, H. Wu, A. Liu, F. Ye, *J Mater Chem C Mater* **2020**, *8*, 12092.

[35] L. Tan, A. C. Davis, D. J. Cappelleri, *Adv Funct Mater* **2021**, *31*, 2007125.

[36] Y. Jian, B. Wu, X. Yang, Y. Peng, D. Zhang, Y. Yang, H. Qiu, H. Lu, J. Zhang, T. Chen, *Supramolecular Materials* **2022**, *1*, 100002.

[37] E. Zhang, T. Wang, W. Hong, W. Sun, X. Liu, Z. Tong, *J Mater Chem A Mater* **2014**, *2*, 15633.

[38] D. Yu, Y. Teng, H. Feng, X. Lin, J. Li, Q. Wang, C. Xue, *RSC Adv* **2022**, *12*, 7898.

[39] P. Sukhavattanakul, H. Manuspiya, *Carbohydr Polym* **2020**, *230*, 115566.

[40] J. Sapkota, S. Kumar, C. Weder, E. J. Foster, *Macromol Mater Eng* **2015**, *300*, 562.

[41] X. Min Dong, J. Ë Ois Revol, D. G. Gray Ã, *Cellulose* **1998**, *5*, 19.

[42] T. Tanaka, D. J. Fillmore, *J Chem Phys* **1979**, *70*, 1214.

[43] A. Peters, S. J. Candau, *Macromolecules* **1988**, *21*, 2278.

[44] M. Zrinyi, J. Rosta, F. Horkay, *Macromolecules* **1993**, *26*, 3097.

[45] K. Cui, C. Yu, Y. N. Ye, X. Li, J. P. Gong, *Proc Natl Acad Sci U S A* **2022**, *119*, e2207422119.

[46] Y. Tan, D. Wang, H. Xu, Y. Yang, X. L. Wang, F. Tian, P. Xu, W. An, X. Zhao, S. Xu, *ACS Appl Mater Interfaces* **2018**, *10*, 40125.

[47] B. W. Chieng, S. H. Lee, N. A. Ibrahim, Y. Y. Then, Y. Y. Loo, *Polymers (Basel)* **2017**, *9*, 355.

[48] K. Pavalaydon, H. Ramasawmy, D. Surroop, *Environ Dev Sustain* **2022**, *24*, 9963.

[49] M. Larsson, A. Johnsson, S. Gårdebjer, R. Bordes, A. Larsson, *Mater Des* **2017**, *122*, 414.

Concluding remarks

In this doctoral thesis, the author constructed functional stimuli-responsive materials consisting of a responsive domain and a supporting network. To achieve high mechanical stability of the networks, thermoresponsive polymers were used as responsive domains, while cellulose was employed as supporting materials. The temperature-dependent functions on the responsiveness of these materials were developed.

In chapter 1, stiffness-changing monolithic materials were fabricated utilizing combination of CM as a supporting network and PSMA as a responsive domain. Two components were combined by facile polymerization of SMA in the presence of the CM. CM exhibited the continuously porous structure, contributing to both the reinforcement and flexibility of the materials. PSMA served as a thermoresponsive polymer, demonstrating the stiffness-changing behavior of PSMA-CM. The resultant monoliths displayed the stiffness-switching behavior in response to temperature. The thermoresponsive stiffness switchability, which was dominated by the properties of PSMA, indicates that the formation of PSMA-cellulose intermingled structure was effective for the responsiveness. In addition, PSMA-CM showed polarity-dependent stiffness change. Moreover, the materials demonstrated shape recoverability and reversible stiffness switching after repeating compression at below and above the melting temperature of PSMA, owing to the stability of CM and thermoresponsive properties of PSMA.

In chapter 2, the thermoresponsive composite hydrogels were constructed from the BC network and PSMA particles. The BC hydrogel network served as the supporting network to enhance the dimensional stability of the materials. The responsiveness was realized by incorporation of PSMA particles into the BC network owing to their sharp phase transition, facilitating excellent stiffness-switching behavior. Also, it is revealed that the size and concentration of PSMA particles affected the PSMA-BC on mechanical properties and stiffness-changing behavior. Increasing amount of PSMA particles with high dispersibility in the network enhanced the variation of stiffness between below and above the phase transition temperature. This is because the PSMA particles effectively acted as reinforcing filler in their stiff state below the melting temperature, while they had the less effect in the soft state above melting temperature.

In chapter 3, thermoresponsive single-layer hydrogel actuators were produced by generating the gradient structure of CNC in PNIPAAm network *via* application of electric field. Gradient

distribution of CNC was controlled by adjusting condition for electrophoresis and preparation of hydrogels, such as electrophoresis time, applied voltage, and amount of CNC. Optimization of these parameters contributed to the high bending rate and angle of the hydrogel actuators. The bending ability was derived from the different deswelling rate along the different density of the CNC particles in the hydrogel network, which was investigated by deswelling kinetics of the composite hydrogels. Furthermore, it is revealed that the bending properties were influenced by dimension of CNC.

In conclusion, the author presented functional stimuli-responsive materials based on morphological control in network structures. The stimuli-responsive materials were constructed by well-controlled morphologies and distribution of both the thermoresponsive polymers and the cellulose-based components to develop the responsive functions from synergistic effects of the combination of them. The cellulose-based components exhibited a substantial supporting effect on the stimuli-responsive materials, as seen by their enhanced mechanical performance, while retaining the properties of the responsive domains. The author postulated that the material designs can contribute to the development of the next generation of sustainable functional stimuli-responsive materials.

List of Publications

1. Shape-Stabilized Monolithic Composite for Switchable Stiffness Based on Cellulose and Poly(stearyl methacrylate)
Nontarin Roopsung, Akihide Sugawara, Yu-I Hsu, Taka-Aki Asoh, and Hiroshi Uyama*
ACS Applied Polymer Materials, **2023**, *5(6)*, 4488.
DOI: 10.1021/acsapm.3c00611

2. Cellulose Nanocrystal-based Gradient Hydrogel Actuators with Controllable Bending Properties
Nontarin Roopsung, Akihide Sugawara, Yu-I Hsu, Taka-Aki Asoh, and Hiroshi Uyama*
Macromolecular Rapid Communications, **2023**, 2300205.
DOI: 10.1002/marc.202300205

3. Switchable Stiffness of Composite Hydrogels Triggered by Thermoresponsive Phase-Change Particles
Nontarin Roopsung, Thuy Le Huynh An, Akihide Sugawara, Taka-Aki Asoh, Yu-I Hsu, and Hiroshi Uyama*
Bulletin of the Chemical Society of Japan, **2023**, *96(7)*, 636.
DOI: 10.1246/bcsj.20230094

Acknowledgements

I am appreciative to both Osaka University and the Japanese government Ministry of Education, Culture, Sports, and Science (MEXT) for permitting me to fulfill graduate studies at Osaka University with financial assistance from MEXT through the 3 years.

Genuinely, I would like to thank my supervisor, Professor Hiroshi Uyama of Osaka University, for his positivity in me and for the experience of working in the Uyama laboratory as a doctoral student from 2020 to 2023. As a researcher, I was able to advance thanks to his encouragement and several opportunities.

I would like to convey my gratefulness to Professor Taka-Aki Asoh of Osaka University, who appointed as my advisor during my first early research projects and gave me the skills. I am obliged to Professor Akihide Sugawara for helping me with the preparation of the thesis and manuscripts and for his instructive comments and recommendations. Particularly, I would like to thank Professor Yu-I Hsu for her encouragement and suggestions whenever encountering impediments. For their informative comments on this thesis, I would also like to convey my gratitude to Professors Hidehiro Sakurai and Masaya Nogi.

I would like to extend my gratitude to everyone who has worked at Uyama Laboratory, both former and current: Yoko Uenishi, Tomoko Shimizu, Dr. Yasushi Takeuchi, Dr. Xinnan Cui, Tanimura Kyoko, Erina Katsuragawa, Chikako Abe, Rieko Yagi, Yasuko Matsuda, Kyoko Fuma.

I would like to express my utmost gratitude to all members who worked in the Uyama laboratory between 2020 and 2023 for hearty supports and kind assistances in research and daily life. Exclusively, I would like to thank to: Dr. Toshiki Tamiya, Dr. Shunsuke Mizuno, Dr. Naharullah Bin Jamaluddin, Dr. Yankun Jia, Dr. Raghav Soni, Dr. Hanyu Wen, Dr. Yanting Lyu, Dr. Yan Wang, Dr. Luwei Zhang, Dr. Meng Wei, Dr. Mark Adam Malaluan Ferry, Madhurangika Panchabashini Horathal Pedige, Yuxiang Jia, Emil Hajili, Manjie He, Yu Cao, Peng Du, Juan Wang, Kazuki Shibasaki, Atsuki Takagi, May Myat Noe, Hasinah Binti Mohamed Rafiq, Judit Rebeka Molnár, Guan Wang, Ying Yao, Ruiqi Zhang, Yihan Gao, Kohei Kikkawa, Airi Ozaki, Jiaxin Alice Chen, Yuya Fujiwara, Yuka Kashihara, Shiho Takai, Yuji Kiba, Takeshi Hiraoka, Yuki Shioji, Atsushi Koizumi, Motoi Oda, Kaita Kikuchi, Koki Tsujita, Hajime Fujimori, Suzune Miki, Thuy Le Huynh An, Izzah Durrati Binti Haji Abdul, Sooyeon Noh, Xinyu Lou, Hiroshi Hasagawa, Shotaro Yano, Kippei Yamamura, Rika Onishi, Hajah Wafiqah Binti Haji Daim, Ziyu

Meng, Shafinee Yarnina Hj Md Shafri, Alejandro Adrian Ayala Escamilla, Daniela Yacine Sebastião Bravo Da Costa, Jiahui Dong, Yuka Asai, Yinxiang Shen, Moe Kominami, Akane Odagaki, Rina Kugimiya, Shunya Kubo, Sota Nakagawa, Maoko Hayashi, Shunsuke Kondo, Yudai Ioku, Naoaki Ishihara, Yuta Okuda, Kanoko Sakai, and Takehiro Masuda.

I am grateful for the support I have received from both local and distant friends; Kulachatr Panyawechamontri, Butsaratip Suwattananurak, Chayanee Wongsuriyanon, Suthinee Attachaipanich, Yuenting Lau, Pacharapaul Lueangratana, Jirawit Jiracheewee, Sirachat Sirilert, Karnkoon Meephark, Thanyaporn Tengsuttiwat, Wisansaya Jaikiandee, Parichat Tawornchat, Chanoknun Boonyaratanasewee, Onnicha Rattanopas, Woraphan Intaphan, Yanawat Manmana, Nitirak Rayabphand, and Phubodee Tuongratanaphan.

Lastly, I would like to express my heartfelt appreciation to my parents, Banjerd and Methinee Roopsung and my brother, Nontapat Roopsung for their thoughtful attention and continuous encouragement.

June 2023

NONTARIN ROOPSUNG